Reliability Engineering and System Safety 122 (2014) 124–144

Contents lists available at ScienceDirect

Reliability Engineering and System Safety

journal homepage: www.elsevier.com/locate/ress

Unsaturated flow modeling in performance assessments for the Yucca Mountain disposal system for spent nuclear fuel and high-level radioactive waste

Rob P. Rechard [a,*], Jens T. Birkholzer [b], Yu-Shu Wu [c], Joshua S. Stein [d], James E. Houseworth [b]

[a] Nuclear Waste Disposal Research & Analysis, Sandia National Laboratories, P.O. Box 5800, Albuquerque 87185-0747, NM, USA
[b] Earth Sciences Division, Lawrence Berkeley National Laboratory, Berkeley 94720, CA, USA
[c] Colorado School of Mines, Golden, CO, USA
[d] Photovoltaic and Distributed Systems, Sandia National Laboratories, Albuquerque 87185-1033, NM, USA

ARTICLE INFO

Available online 4 July 2013

Keywords:
Unsaturated fluid flow
High-level radioactive waste
Spent nuclear fuel
Radioactive waste disposal
Performance assessment
Yucca Mountain

ABSTRACT

This paper summarizes the progression of modeling efforts of infiltration, percolation, and seepage conducted between 1984 and 2008 to evaluate feasibility, viability, and assess compliance of a repository in the unsaturated zone for spent nuclear fuel and high-level radioactive waste at Yucca Mountain, Nevada. Scientific understanding of infiltration in a desert environment, unsaturated percolation flux in fractures and matrix of the volcanic tuff, and seepage into an open drift in a thermally perturbed environment was initially lacking in 1984. As understanding of the Yucca Mountain disposal system increased through site characterization and *in situ* testing, modeling of infiltration, percolation, and seepage evolved from simple assumptions in a single model in 1984 to three modeling modules each based on several detailed process models in 2008. Uncertainty in percolation flux through Yucca Mountain was usually important in explaining the observed uncertainty in performance measures: cumulative release in assessments prior to 1995 and individual dose, thereafter.

1. Introduction

Understanding the movement of water through porous and fractured volcanic tuff in the unsaturated zone (UZ) was a challenging scientific endeavor of the Yucca Mountain Project (YMP). This paper presents the progression of changes in modeling of infiltration at the surface, percolation through the mountain, and seepage into the repository drifts since 1984 to provide a historical perspective on the performance assessment (PA) for the 2008 license application (PA–LA), which is summarized in this special issue of *Reliability Engineering and System Safety.* PA–LA underlies the Safety Analysis Report (SAR/LA) submitted to the US Nuclear Regulatory Commission (NRC) in 2008 by the US Department of Energy (DOE) for constructing a repository at Yucca Mountain (YM) for high-level radioactive waste (HLW), commercial spent nuclear fuel (CSNF), and spent nuclear fuel owned by DOE (DSNF) (Fig. 1) [1,2]. Companion papers provide a historical summary of site selection and regulatory development by the US Environmental Protection Agency (EPA) and NRC [3]; hazards and scenarios identified [4]; repository design and site characterization conducted by YMP [5,6]; evolution of other models of the YM disposal system [7–9]; and past results [10].

The general progression of PA analysis and results of sensitivity analysis have been described by noting the changes in linkages of modules $\mathcal{M}^{\beta}$ for phenomena at spatial location β of the exposure pathway/consequence model $\mathcal{R}(\sim)$ [7] (Fig. 2). However, discussion of some of the assumptions, simplifications, and implementation within the various modules, as presented here for infiltration ($\mathcal{M}^{Infil}$), UZ percolation ($\mathcal{M}^{UZflow}$), and seepage into the repository ($\mathcal{M}^{Seep}$), is necessary to understand the information flowing through the linkages. These details help the reader get a glimpse of the complexity and the challenge of combining numerous simplified models in a PA simulation. A summary of the resulting empirical equations underlying the models is also necessary in order to define the parameters that were identified in sensitivity analysis as important in explaining the variation in performance measures (cumulative release R prior to 1998 and individual dose $D(t)$, thereafter) [10].

Large scale risk analysis must usually be conducted in several iterations to refine and focus the analysis on those aspects most pertinent to the policy issue [11, Fig. 3.2], and this iterative approach has indeed occurred at YMP. Seven PAs provide historical markers for the evolution of $\mathcal{M}^{Infil}$, $\mathcal{M}^{UZflow}$, and $\mathcal{M}^{Seep}$. Four early PA iterations to evaluate feasibility of the YM disposal system are discussed: a deterministic evaluation of the disposal

* Corresponding author. Tel.: +1 505 844 1761; fax: +1 505 844 2348.
E-mail address: rprecha@sandia.gov (R.P. Rechard).

0951-8320/$ - see front matter
http://dx.doi.org/10.1016/j.ress.2013.06.025

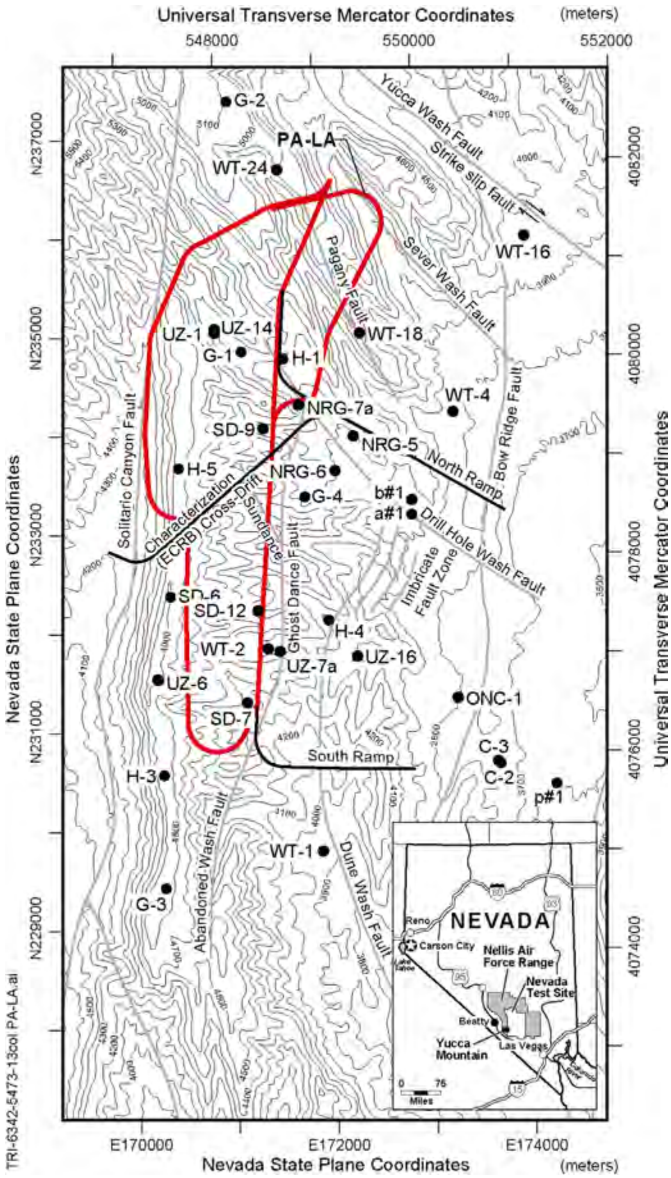

Fig. 1. Repository layout for PA–LA and pertinent wells at Yucca Mountain, Nevada.

system to support the draft and final environmental assessment of Yucca Mountain for further characterization, PA–EA [12,13]; the first stochastic simulation, PA-91 [14]; and two evaluations to provide guidance on repository design options, PA-93 [15] and PA-95 [16]. These four early PAs were followed by three PAs to support major decisions: a viability assessment, PA–VA, in 1998 [17]; an analysis for the site recommendation, PA–SR, in 2000 [18]; and the licensing application analysis, PA–LA, in 2008 [1,2].

2. UZ modeling for PA–EA

PA–EA was conducted to support the environmental assessment of the site for further characterization [6; 7, Appendix A; 10, Table 1]. In PA–EA, CSNF in 33,000 small, thin-walled stainless steel containers was placed either vertically in the floor or horizontally in pillars of rooms [5]. Catastrophic failure of the container was assumed to occur exponentially or at a fixed time between 300 and 1000 years [8]. Cumulative, normalized

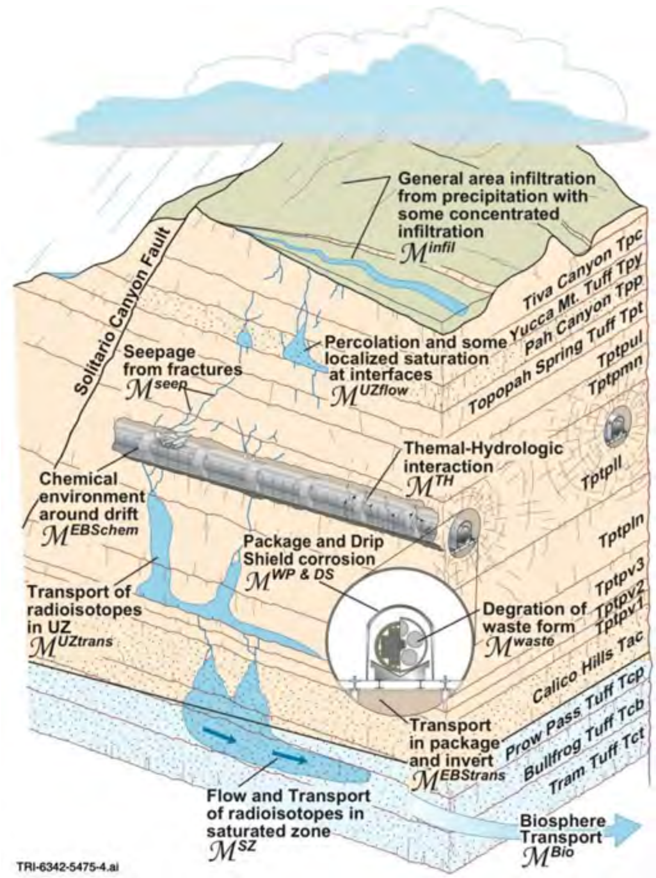

Fig. 2. Conceptualization of water and radionuclide movement and corresponding eleven modeling modules of PA-VA, PA-SR, and PA-LA at Yucca Mountain for the undisturbed scenario class.

release ($R_U^{84}(\mathbf{e}^e)$) over 10^4 years to the accessible environment boundary 10 km from the repository (x^{ae}), the performance measure proposed in the draft EPA radiation protection standard 40 CFR 191 [3], was evaluated for the undisturbed scenario ($\mathcal{A}_U$) along a groundwater pathway as

$$R^{84}_{U,gw}(\mathbf{e}^e) = \sum_{r=1}^{n_U^r=17} \frac{1}{L_r f_{mass}} \int_0^{10^4\ \mathrm{yr}} \mathcal{R}_{U,gw,r}(t;\mathbf{e}^e)\Big|_{x^{ae}=10\ \mathrm{km}} dt \qquad (1)$$

where f_{mass} is the mass fraction of metric tons of heavy metal (MTHM) in the repository (MTHM/10^3 MT); L_r is the limiting value specified in 40 CFR 191 for radionuclide r; $\mathbf{e}^e$ is an ordered nE-tuplet of epistemic model parameters, $\boldsymbol{e}=\{\varphi_1,..., \varphi_n,...\varphi_{nE}\}$, which for PA–EA were deterministically varied; and $\mathcal{R}_{U,gw,r}(\sim)$ is the exposure pathway/consequence model for $\mathcal{A}_U$ that calculates the flux across a boundary. The consequence model $\mathcal{R}_{U,gw,r}(\sim)$ consisted of two model components for radionuclide transport in a single code [9]: (1) transport in fractures and matrix of the UZ ($\mathcal{M}^{UZ}$), and (2) transport in the matrix of the SZ ($\mathcal{M}^{SZ}$).

2.1. UZ percolation at repository horizon in PA–EA

Water percolation from the surface to the repository horizon was not simulated in PA–EA (although preliminary work had been conducted [19,20]). Rather, percolation at the repository level (q^{perc}) was set at 0.1 and 0.5 mm/yr for current conditions and at 5 and 20 mm/yr for a pluvial climate sometime in the future in *Ceterus parabis* sensitivity studies (i.e., q^{perc}∼0.1, 0.5, 5, 20 mm/yr in precursor to $\mathcal{M}^{UZflow}$) [12, Table 8]. Although the model of regional water balance showed that no recharge was necessary at Yucca Mountain to explain flow patterns [21], the lower bound for current conditions was based on measurements of hydraulic conductivity for the matrix (K_m) on the order of 0.1 mm/yr.[1]

The upper value of 0.5 mm/yr for current conditions was based on a 1984 US Geological Survey (USGS) conceptual model and simulations by Sandia National Laboratories (SNL). The USGS had recently proposed that infiltration from the surface was diverted laterally at the interface between the Paintbrush (PTn) and Topopah Spring tuff (TSw1) hydrologic units above the repository such that only 0.5 mm/year percolated through the repository area [6, Appendix A; 22; 23] (Fig. 3). Also, SNL simulations showed that 0.5 mm/yr was the maximum flux that could occur and still match the observed partial saturation between 0.5 and 0.7 [12].

The lower bound for pluvial conditions used a previous 1983 USGS conceptual model that proposed, based on observations of outcrops, that sufficient fracturing existed in the tuffs such that percolation at the repository horizon would equal infiltration (i.e., set between 4.5 and 6.0 mm/yr and precursor to $\mathcal{M}^{Infil}$) [6, Appendix A; 23] (Fig. 4). The upper value of 20 mm/yr was thought bounding because substantial increase in precipitation was not anticipated during a climate change in the first 10^4 years since Yucca Mountain was in the rain shadow of the Sierra Nevada and Transverse Ranges [6,12].

2.2. Fraction of percolation diverted as seepage in PA–EA

Tests on water-migration around small heaters (to simulate HLW canisters) began in 1980 in G-tunnel near Yucca Mountain [6, Appendix A; 25]. However for simplified modeling in PA–EA, the thermal evolution near the emplacement drift was not considered for seepage. Rather, ambient percolation was assumed to begin after a short thermal period of 300 years that corresponded with the first breach of a waste container (i.e., $\tau^{fail}=300$ years). The amount of percolation that became seepage was the product of the percolation over the repository area and fraction of percolation diverted as seepage to the drifts and packages (f^{perc} in precursor to $\mathcal{M}^{Seep}$).

The f^{perc} was set at 0.0025, 0.025, or 0.25, based on simple geometric arguments [12]. The high diversion fraction of 0.25 was based on the fact that mining of drifts for floor emplacement would remove about 25% of the rock and that all of this area would contribute to seepage.[2] The medium fraction of 0.025 and low fraction of 0.0025 were based on the fact that boreholes for horizontal waste emplacement in the pillars and boreholes for vertical waste emplacement in the floors would consist of 2.5% or 0.25% of the total repository area, respectively.

3. UZ Modeling for PA-91

PA-91 was conducted in 1991 to demonstrate site feasibility [7, Appendix A; 10, Table 1; 14]. CSNF was placed in a package and repository of similar design to PA–EA, but as specified in the 1988 Site Characterization Plan (SCP) [5]. In addition to evaluating release of ^{14}C at the surface, the expected cumulative, normalized release via a groundwater pathway ($\overline{R}^{91}_{j,gw,acm}$) over 10^4 years was evaluated at a 5-km boundary (x^{ae}) for 3 scenario classes [4, Table 1; 7]: undisturbed—$\mathcal{A}_U$, human intrusion—$\mathcal{A}_H$, and volcanic eruption —$\mathcal{A}_{VE}$, (i.e., $j \sim U,H,VE$). The complementary cumulative distribution

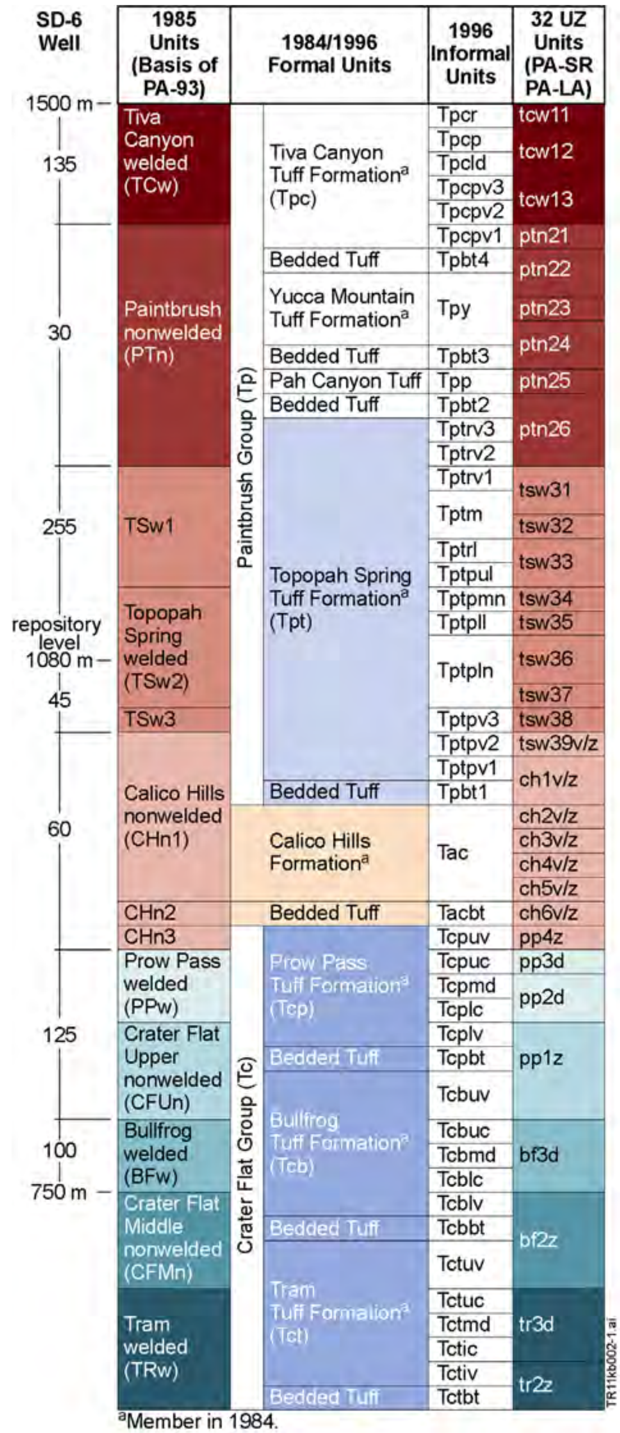

Fig. 3. Formal/informal stratigraphy and modeling layers of Yucca Mountain [1, vol. GI Fig. 5-30 and Table 5-30 and Chapter 2, Table 2.3.2-2; 15, Figs. 6 and 7].

function (CCDF) for $\mathcal{A}_U$ along the groundwater pathway ($\overline{R}^{91}_{U,gw,acm}$) from the releases in the UZ and SZ for the transport of 9 radionuclides ($n^r_U=9$) was evaluated using Latin Hypercube Sampling (LHS—a form of Monte Carlo integration to determine the expectation) with either 1800 or 1000 samples (n_U^{LHS}) [7, Eqs. (4) and (5)]

$$\overline{\wp}\left\{\overline{R}^{91}_{U,gw,acm} > R\right\} = \frac{1}{n_U^{LHS}} \sum_{\ell=1}^{n_U^{LHS}} \mathcal{H}\left\{ \sum_{r=1}^{n^r_U=9} \frac{1}{L_r f_{mass}} \int_0^{10^4\,\mathrm{yr}} \mathcal{R}_{U,gw,r,acm}(t;\mathbf{e}^e)\Big|_{x^{ae}=5\ \mathrm{km}} dt - R \right\} \qquad (2)$$

[1] This observation would not change for the next 24 years. At the site scale, PA–LA continued to show no noticeable recharge to the regional flow system in the SZ at Yucca Mountain [9, Fig. 9].

[2] This approach ignores the capillary forces that tend to divert percolation around the opening such that only a small faction actually becomes seepage. PA-91 would make a more sensible approximation, but capillary forces were not theoretically accounted for until PA–VA.

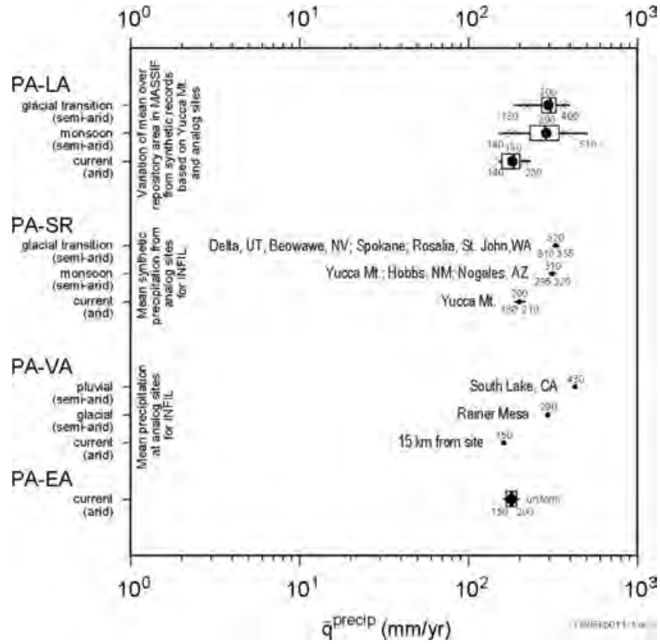

Fig. 4. Comparison of precipitation as function of climate states in PAs for Yucca Mountain [12; 17, p. 3-14; 18, Table 4-11; 24, Fig. 7.13-1].

where $\mathcal{H}(x)=0$ if $x\le 0$; $\mathcal{H}(x)=1$ if $x>0$ and the derivation explained elsewhere [7, Appendix B].

Although eventually 11 modules would be used (Fig. 2), four modeling modules $\mathcal{M}_j^{\alpha}$ were used for the consequence model ($\mathcal{R}_{U,gwr,acm}$) in PA-91: (1) flow in the UZ ($\mathcal{M}_j^{UZFlow}$); (2) waste degradation in the engineered barrier system of the repository (*EBS*) ($\mathcal{M}^{Waste}$) [26]; (3) transport in the underlying natural barrier in the *UZ* ($\mathcal{M}_j^{UZtrans}$) [9]; and (4) flow/transport in the natural barrier in the saturated zone (*SZ*) ($\mathcal{M}^{SZ}$) [9]. Two alternative conceptualizations (i.e., *acm*) in $\mathcal{M}^{UZFlow}$ for $\mathcal{R}_{U,gw,r,acm}(t;\mathbf{e}^e)$ were evaluated as described in the next section.

3.1. Percolation at repository horizon in PA-91

Percolation in PA-91 was based on the 1984 USGS conceptual model that assumed substantial lateral flow to faults above the TSw repository tuff (and as modeled with detailed two-dimensional (2-D) UZ flow calculations e.g., [27]), which limited percolation at the repository horizon. The mean value of percolation ($\bar{q}^{perc}$) 10 m above the repository was set at 1 mm/yr (i.e., the surface and most of the UZ above the repository was not modeled—Fig. 2). Because the possible uncertainty of this mean percolation was not known, an exponential distribution (in accordance with the maximum entropy formalism [28]) was selected and sampled during each realization P_f^{cap} of PA-91 ($\bar{q}_\ell^{perc}$). Exponential uncertainty about the mean of 1 mm/year was thought sufficient to account for current, arid conditions and future, semi-arid conditions due to climate change over the 10^4-years simulation period, based on 40 CFR 191 [14, p. 3–19] (Fig. 5). As in PA–EA, ambient percolation was assumed to begin after 300 years ($\tau^{fail}=300$ years); however, for PA-91, resaturation of the matrix surrounding a package was assumed to take 1000 years, as a rudimentary acknowledgment of the thermal period [8].

For evaluating transport below the repository, a flow field was necessary, particularly the partition of flow between fractures and matrix. For PA-91, $\mathcal{M}^{UZflow}$ consisted of six 1-D columns along a cross-section between H-5, G-4, and UE-25a#1 from 10 m above the repository to the water table ~240 m below the repository [14, Table 4-3, Fig. 4-17] (Fig. 1). Five layers were modeled [9, Fig. 5] (Fig. 6): Topopah Springs welded tuff (TSw) for the repository, Topopah Springs vitrophyre (TSv), Calico Hills non-welded vitric tuff (CHnv), a composite zeolitic layer, and a composite welded tuff aquifer layer. Thus, lateral flow below the repository was not evaluated. Two alternative conceptualizations of flow were modeled: the equivalent continuum model (ECM), incorporated into TOSPAC, under development since 1985 [33], and a weeps model, WEEPTSA [14].

3.1.1. Equivalent continuum model (ECM)

The ECM formulation derives composite functions to describe behavior of a fractured rock with a low-permeability matrix as a single continuum (such as functions between unsaturated hydraulic conductivity and liquid saturation and between matrix potential and liquid saturation) [20,34]. For the ECM formulation, TOSPAC calculated a composite velocity field ($\mathbf{q}_{ECM}^{perc}(\mathbf{x})$) based on Richard's equation, which assumes isothermal conditions for a single mobile water phase (i.e., a nonmoving gas phase) [20; 33, Eq. (2.1-25); 35, Eq. (2.80)]

$$C(\mathbf{x};\psi)\frac{\partial\psi(\mathbf{x},t)}{\partial t}=\nabla\bullet(\mathbf{K}_{\mathrm{ECM}}(\mathbf{x};\psi)\bullet\nabla(\psi(\mathbf{x}+t)+z)) \tag{3}$$

where $C(\mathbf{x};\psi)=\partial\theta(\mathbf{x};\psi)/\partial\psi$ and $\theta(\mathbf{x};\psi)$ is the water content. For PA-91, only a 1-D version of Eq. (3) was used, but the full 3-D version was used by PA-VA.

For all PAs, a quasi steady state flow fields were calculated; hence, the left-hand side of Eq. (3) is zero and $\psi\equiv\psi(\mathbf{x})$. Furthermore using Darcy's law with $\mathbf{q}_{ECM}^{perc}(\mathbf{x})=-\mathbf{K}_{\mathrm{ECM}}(\mathbf{x},\psi)\bullet\nabla(\psi(\mathbf{x})+z)$ [14, Eq. (4.43)]

$$0=\nabla\bullet\mathbf{q}_{ECM}^{perc}(\mathbf{x}) \tag{4}$$

where $\mathbf{q}_{ECM}^{perc}$ is the percolation Darcy velocity and the sum of the fracture and matrix Darcy velocities $\mathbf{q}_f^{perc}+\mathbf{q}_m^{perc}$; $\mathbf{K}_{ECM}$ is the composite hydraulic conductivity tensor and equal to $\mathbf{K}_m$+$\mathbf{K}_f$ and where $\mathbf{K}_m$ is the product of intrinsic permeability tensor, relative permeability, liquid density, and inverse of liquid viscosity ($\mathbf{k}_m k_m^{rel}\rho g/\mu$); and ψ is the pressure head and equal to sum of elevation and pressure head (pressure divided by liquid density and gravity constant or $P/\rho g$). The commonly used hydraulic head is the sum of the pressure head and distance above a reference height such as water table ($H=z+\psi=z+P/\rho g$). Other relationships were the composite volumetric moisture content θ_{ECM} and equal to composite of the fracture and matrix saturations (i.e., $\phi_m s_m^{sat}+\phi_f s_f^{sat}\approx\phi_m s_m^{sat}$) and the composite porosity, $\phi_m+\phi_f\approx\phi_m$. In solving Eq. (4) in PA-91, the percolation flux 10 m above the repository was set at the sampled percolation ($\bar{q}_\ell^{perc}(x=10\text{ m})$).

For PA-91 and the other early PAs, the van Genuchten formulation for unsaturated soils was used to define the relative permeability (k_Ω^{rel}) [33, Eq. (2.1-21)]:

$$k_{r\Omega}=(s_\Omega^{eff})^{1/2}[1-(1-(s_\Omega^{eff})^{1/m_\Omega})^{m_\Omega}]^2 \tag{5}$$

$$P_\Omega^{cap}=\frac{1}{\alpha_\Omega^{van}}[(s_\Omega^{eff})^{-1/m_\Omega^{van}}-1]^{1-m_\Omega^{van}} \tag{6}$$

$$s_\Omega^{eff}=\frac{s_\Omega-s_\Omega^{res}}{1-s_\Omega^{res}} \tag{7}$$

where Ω represents either the matrix or fracture domain (i.e., $\Omega\sim m$ or f), and the 12 hydrologic properties to be assigned for each layer or grid block of the model in PA-91 were 6 matrix and 6 fracture properties [36, Section 3.3.3, Table 4-4], van Genuchten air-entry parameter (α_m and α_f), van Genuchten fitting parameter (m_m and m_f), residual liquid saturation (s_m^{res} and s_f^{res}), vertical

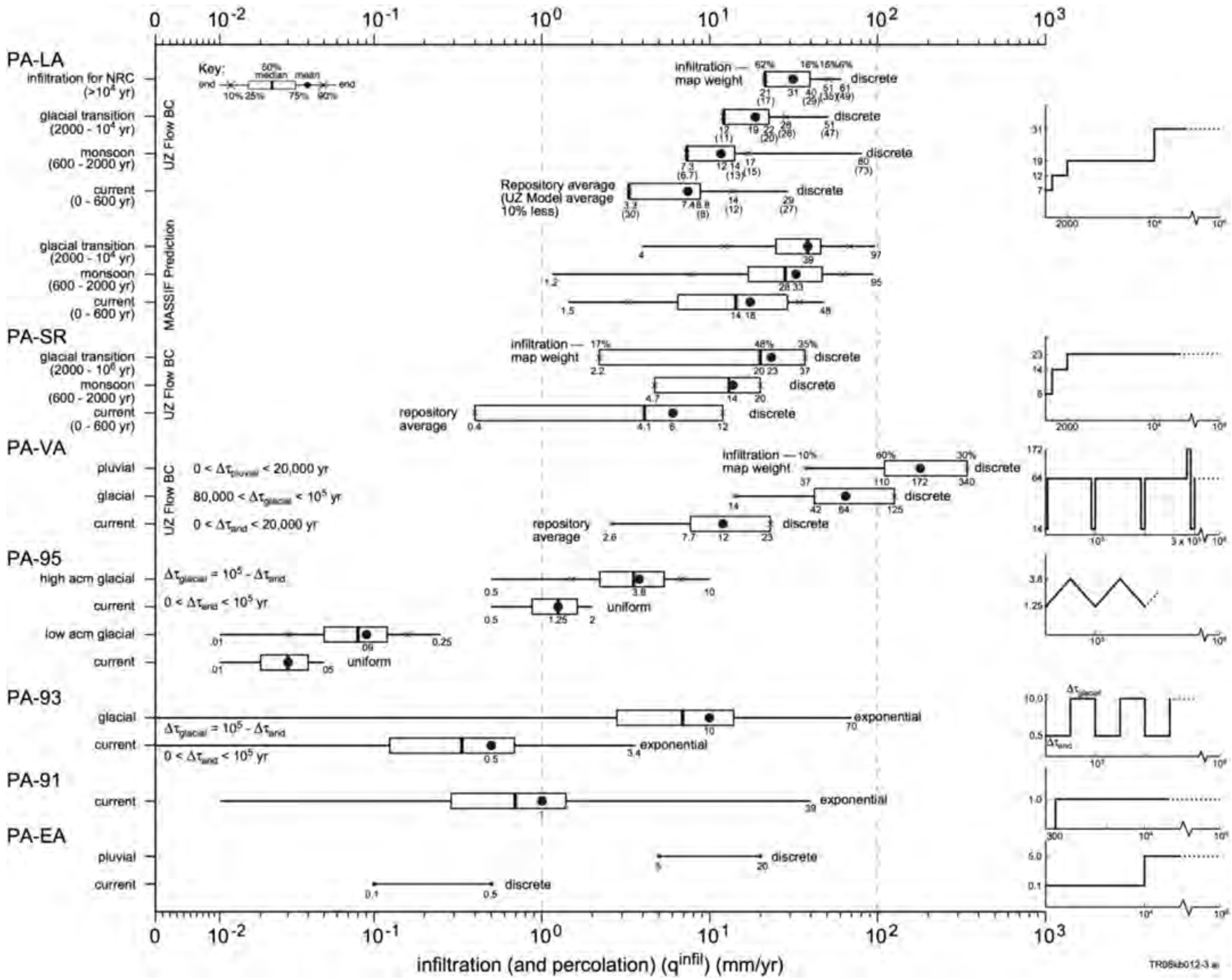

Fig. 5. Infiltration at surface and percolation at repository horizon prior to PA–VA as a function of climate states. High infiltration usually considered for a portion of the regulatory period in YMP PAs [17, Fig. 4-21, Table 3-5; 18, Table 3.2-2; 24, Tables 6.5.7.1-2, 6.5.7.2-2 and 6.5.7.3-2; 29, Fig. 3.7-12; 30, Figs. 2-105–2-107; 31, Tables 6.1-2, 6.1-3 and 6.6-9–6.6-13; 32].

permeability ($k_{m,z}$ and $k_{f,z}$). porosity (ϕ_m and ϕ_f), and saturation (s_m^{sat} and s_f^{sat} for calculating pore velocity, e.g., $v_f^{UZ}(t) = q_f^{UZ}(t)/s_f^{sat}\phi_f$).

The fundamental assumption of the ECM formulation is that there is local equilibrium between the fracture and matrix pressure heads (i.e., $\psi_m = \psi_f$). The advantage of the ECM formulation is that it reduces the number of highly nonlinear equations solved at a grid block from two (one each for the fracture and matrix) to one equation for the composite material. The ECM formulation was not used for UZ flow calculations after PA-95. However, Richard's equation was used for mountain-scale UZ flow through PA–LA.

3.1.2. Weeps conceptual model

The ECM theory assumes that flow is predominately in the tuff matrix until the matrix nearly fully saturates. Because the tuff matrix was not saturated at Yucca Mountain, the theory suggested that infiltration must be low with little fracture flow; hence, radionuclide release would be primarily via diffusive transport to the tuff matrix. Yet by PA-91, enough circumstantial evidence had accumulated to indicate that water flowed down fractures for large distances, consistent with the earlier 1983 USGS conceptual model of flow at Yucca Mountain [6]. Hence, an alternative conceptual weeps model was developed (WEEPTSA), which assumed predominantly fracture flow decoupled from matrix flow [37, p. 891–8]. WEEPTSA was not a process model but rather a series of assumptions. In WEEPTSA, only advective water flow passed through the waste package (WP) and then through the fractures and, thus, was important to determining releases to the accessible environment.

3.2. Estimated seepage into drifts in PA-91

Seepage into a drift is uncertain and spatially varying; yet, YM PAs did not model individual packages. Hence, seepage was expressed statistically in PA-91 and thereafter. While all packages experienced seepage in PA–EA, only a fraction of packages experienced seepage in PA-91. Furthermore, with the ECM formulation, most liquid movement occur in the matrix and so the drift seepage (q_{ECM}^{seep}) and the fraction of packages with drips (f_{ECM}^{WPdrip}) were analytically estimated for each LHS sample ℓ for the ECM formulation as follows [14, Eqs. (4.1) and (4.4); 38]:

$$q_{ECM,\ell}^{seep} = \frac{\overline{q}_\ell^{perc}(x=10m)}{2f_{ECM}^{WPdrip}}\,\mathrm{erfc}\left(\frac{\ln\overline{q}_\ell^{thres} - \mu_\ell^{\mathrm{percvar}} - \sigma_{\mathrm{percvar}}}{\sqrt{2}\sigma_{\mathrm{percvar}}}\right) - \overline{q}_\ell^{thres} \tag{8}$$

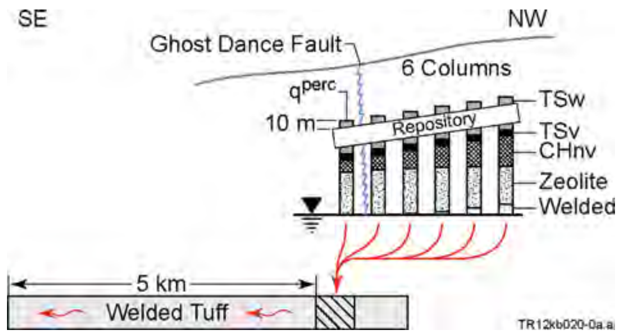

Fig. 6. For PA-91, UZ flow was evaluated in 6 columns, with up to 5 layers that started 10 m above the repository horizon [14, Figs. 4-18 and 4-30].

$$f^{WPdrip}_{ECM,\ell} = \wp\left\{\overline{q}^{perc}_{\ell}(x=10\text{ m}) > \overline{q}^{thres}_{\ell}\right\} = \frac{1}{2}\,\mathrm{erfc}\left(\frac{\ln\overline{q}^{thres}_{\ell} - \sigma_{\text{percvar}}}{\sqrt{2}\sigma_{\text{percvar}}}\right) \tag{9}$$

where $\overline{q}^{perc}_{\ell}(x=10\text{ m})$ was the mean percolation 10 m above the repository (for each LHS sample $\sigma^{Q^{seep}}(q^{perc})$ from an exponential distribution representing uncertainty as described above in Section 3.1), and $\overline{q}^{thres}_{\ell}$ was the threshold percolation when water moves through the fractures allowing seepage. The uncertainty in $\overline{q}^{thres}_{\ell}$ was expressed by an exponential distribution with a mean set at the mean matrix hydraulic conductivity of the repository horizon ($\overline{K}^{TSw}_{m} = 2\times10^{-11}$ m/s). Note that the seepage q^{seep}_{ECM} was increased above percolation $\overline{q}^{perc}_{\ell}(x=10\text{ m})$ by the fraction of packages with drips (f^{WPdrip}_{ECM}) to account for flow focusing.

The $\mu^{\text{percvar}}_{\ell}$, the mean of the log transform of the spatial variability of percolation, and $\sigma_{percvar}$, the standard deviation of the log transform of the spatial percolation in Eqs. (8) and (9), were determined by assuming a lognormal distribution for spatial variability in percolation; that is, by definition for a lognormal distribution[3]

$$\overline{q}^{perc}_{\ell}(x=10m) = \exp\left\{\mu^{\text{percvar}}_{\ell} + \frac{1}{2}\,\sigma^{2}_{\text{percvar}}\right\} \tag{10}$$

$$\upsilon^{2}_{perc} = \left(\frac{\sigma_{perc}}{q^{perc}}\right)^{2} = \exp\left\{\sigma^{2}_{\text{pervar}}\right\} - 1 \tag{11}$$

where υ_{perc}, the coefficient of variation of the spatial percolation, was set to 1.3 for PA-91. Much effort would be expended in PA–VA and later PAs to replace Eqs. (8)–(11) with a numerical modeling basis.

For the weeps model, the seepage flux and the number of weeps (n_{weeps}) were expressed as [14, Eqs. (4.47) and (4.48)]

$$q^{seep}_{weep} = \hbar((2b_f)^3, w_f) \tag{12}$$

$$n_{\text{weeps}} = \frac{A^{rep}\overline{q}^{perc}f^{connect}}{q^{seep}_{weep}b_f w_f f^{fracflow}} \tag{13}$$

where $2b_f$ is the flowing fracture aperture (loguniformly distributed between 10^{-5} and 10^{-3} m and important for PA-91 and PA-93 [10, Table 2]), w_f is the horizontal fracture width (uniformly distributed between 0.01 and 1 m), $f^{connect}$ is fraction of fractures with pathways from the surface to the water table (uniformly distributed between 0 and 1), A^{rep} is the area of the repository (5.61×10^{6} m^2) [5, Table 1], and $f^{fracflow}$ is fraction of time in a year that the fracture flows (episodicity) and loguniformly distributed between 1/365 and 100/365). The $f^{fracflow}$ was an important parameter for PA-91 [10, Table 2].

4. UZ flow modeling for PA-93

YMP conducted PA-93 to provide guidance on characterizing the site and two options for package packing to create to heat loads (14 and 28 W/m^2) and two options for package orientation in the repository (vertical and in-drift) [7, Appendix A; 10, Table 1; 15]. For vertical emplacement, CSNF was in 9.5 mm thick containers of Alloy 825; for in-drift emplacement, CSNF was in double layered containers of 100-mm steel and 9.5-mm Alloy 825 [5, Tables 2 and 3]. Two performance measures were evaluated at a 5 km boundary of accessible environment (x^{ae}) [3, Table 4]: (a) the summed normalized release at 10^4 years (Eq. (2)), and (b) dose from drinking contaminated water (D^{93}_{Ugw})) evaluated over 10^6 years. The summed normalized release was evaluated for 3 scenarios classes: $\mathcal{A}_U$, $\mathcal{A}_H$, igneous activity $\mathcal{A}_V$ where the latter included the igneous intrusion subclass $\mathcal{A}_{VI}$ and the volcanic eruption $\mathcal{A}_{VE}$. Dose was only evaluated for $\mathcal{A}_U$. As in PA-91, both a groundwater and gaseous pathway in the UZ were evaluated for $\mathcal{A}_U$ using an ECM or weeps model formulation. For PA-93, a CCDF of the maximum expected doses ${}^{\max}D_{Ugw}$from 7 transported radionuclides was calculated at the 5-km boundary for $t<10^6$ years as [7, Eq. (13)]

$$\wp\left\{{}^{\max}D^{93}_{Ugw,acm} > D\right\} = \mathcal{H}\left\{\left[\sum_{r}^{n^r_U=7}\frac{f^{BDCF}_{U,r}}{Q^{indv}_{93,\ell}}\mathcal{R}_{Ugw,r,acm}(t;\mathbf{e}^{e}_{\ell})\right]_{x^{ae}=5\text{ km}} - D\right\} \text{ for } \ell=1,\ldots,n^{LHS}_{U} \tag{14}$$

4.1. Climate change and infiltration in PA-93

PA-93 switched to a 10^{-6} yr simulation based on preliminary discussions of the National Academy of Science (NAS) on a site-specific regulation for a repository at Yucca Mountain [3]. Hence, climate fluctuations were thought important to model. For PA-93, net infiltration beyond the evapotranspiration zone near the surface (q^{infil}) was assumed to be exponentially distributed, similar to percolation in PA-91, but two climates were specified: an interglacial, arid condition with a mean of 0.5 mm/yr and a glacial, semi-arid condition with a mean of 10 mm/yr. The period for one cycle of arid and glacial climate was fixed at 10^5 years (i.e., $\Delta\tau_{glacer}+\Delta\tau_{arid}=10^5$). The duration of the arid period ($\Delta\tau_{arid}$) was uniformly distributed between 0 and 10^5 years and an important parameter for PA-93 [10, Table 2]. Climate change ($w(t)$) was incorporated in PA-93 as a jump from one steady-state condition to another [15, Section 14.3] (Fig. 5); thus, q^{infil} was a function of time through the climate change $w(t)$.

4.2. Percolation at repository in PA-93

In PA-93, geostatistical methods were used to simulate ten 3-D stratigraphic models that were consistent with all the well data available at the time [15, Section 6]. Yet, because of time constraints, the uncertainty represented by these ten simulations was not included in the PA-93. For the ECM formulation, one of the simulations was selected and flow in the UZ below the cool (14 W/m^2) repository footprint was modeled through 8 columns with 5 northwest and 3 southeast of the access drifts at the Ghost Dance Fault (rather than 6 columns as in PA-91) (Fig. 7) [15, Fig. 14-5; 33]. The 5 columns northwest of the access drifts were used to model the hot (28 W/m^2) repository footprint. Each column

[3] Models of the UZ above the repository horizon in PA–VA [30, Figs. 2-105 to 2-107, PA–SR 29, Fig. 3.7-12, and PA–LA 39, Figs. 6.6-9–6.6-13] confirmed that percolation was spatially distributed fairly log-normally across the repository.

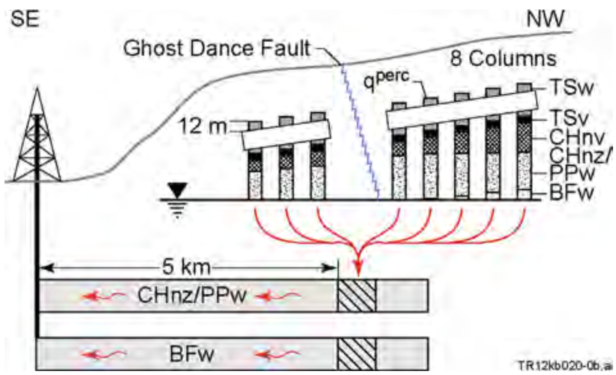

Fig. 7. For PA-93, UZ flow was evaluated in up to 8 columns, with up to 5 layers that started 12 m above the repository horizon [15, Figs. 7-1 and 11-1].

started 12 m (rather than 10 m as in PA-91) above the repository and extended to the water table. As with PA-91, up to 5 layers were modeled but the composition of the bottom 2 layers differed [9, Fig. 6; 15, Table 7-23 Fig. 14-5]: Topopah Spring welded tuff (TSw), Topopah Spring vitrophyre (TSv), a combined Calico Hills (CHnv), Calico Hills nonwelded zeolitic/Prow Pass welded tuff (CHnz/PPw), and Bull Frog welded tuff (BFw).

In PA-93, percolation 12-m above the repository was set equal to the infiltration flux for the weeps model (i.e., $q^{perc}_{weep,\ell}(t, x=12\text{ m}) = q^{infil}_{\ell}(t)$), consistent with the 1983 USGS conceptual model of sufficient fracture flow throughout the mountain. For the ECM formulation, the infiltration flux was adjusted to determine the percolation whenever $q^{infil}_{\ell} > K^{TSw}_{m,\ell}$ as follows [15, Chapter 8]:

$$\begin{aligned}\bar{q}^{perc}_{ECM,\ell}(t,x=12\text{ m}) &= \bar{q}^{infil}_{\ell}(t) \text{ if mean } \bar{q}^{infil}_{\ell}(t) < K^{TSw}_{m,\ell}\text{ ;} \quad \text{otherwise}\\ &= K^{TSw}_{m,\ell}\text{ }, \wp = 0.5; \quad \text{otherwise}\\ &= -K^{TSw}_{m,\ell}\ln(1-U^{perc}_{\ell}[0,1]), \wp = 0.5 \end{aligned} \tag{15}$$

where $U^{perc}_{\ell}[0,1]$ was a uniformly distributed random variable between 0 and 1 such that q^{perc}/K^{TSw} was exponentially distributed, with a mean of matrix hydraulic conductivity for the host rock ($K^{TSw}_{m,\ell}$), in 50% of the samples whenever the variable $q^{infil}_{\ell}(t) > K^{TSw}_{m,\ell}$. The distribution of $K^{TSw}_{m,\ell}$ included a much larger range than in PA-91, based on a measurement from an additional well (0 to 20 mm/yr versus 0 to 5 mm/yr) [40, Fig. 8-6] and was an important parameter for PA-93; yet, the probability model for the ECM formulation expressed in Eq. (15) resulted in much reduced fracture percolation in the TSw (only 18% of the simulations under a dry climate, and 40% of the simulations under a wet climate had fracture flow) [40, Figs. 8 and 9].

4.3. Estimated seepage into drifts in PA-93

Emplacement of waste directly in the drift in PA-93 and consideration of two different thermal load options increased the importance of evaluating the process of seepage entering the drift. Of several important phenomena (e.g., capillarity) and features (e.g., heterogeneous permeability) that influence seepage, thermal effects were considered first. The thermal load for the repository design in PA-91 was 14 W/m². In addition to this base case, another option considered for PA-93 was to double the base value to 28 W/m² to produce an entire repository zone at temperatures above boiling for many hundreds of years compared to a few hundred years for 14 W/m². A new thermal module ($\mathcal{M}^{T}$) for PA-93 roughly modeled the expansion and contraction of this heated zone [8]. From the temperature isotherms ($<96\,^{\circ}$C), $\mathcal{M}^{T}$ estimated, as a function of time, (1) the moisture displaced as the repository heated ($q^{therm}(t)$), and (2) the fraction of the repository that was without liquid water ($f^{dry}(t)$). In turn, $\mathcal{M}^{UZflow}$ estimated the effective percolation at the repository horizon for both the ECM and weep alternative conceptual models ($acm \sim ECM, weep$) [15, Eq. (10.2)] as

$$\bar{q}^{eff}(t) = \frac{\bar{q}^{perc}(t)}{1-f^{dry}(t)} + q^{therm}(t) \tag{16}$$

where the first term is the ambient percolation above the repository that is diverted to the cooler portion of the repository.[4] After, the thermal period $f^{dry}=0$ and $q^{therm}=0$; hence, $\bar{q}^{eff} = \bar{q}^{perc}$.

For the weeps model, the seepage flux q^{seep}_{weep} and number of weeps n_{weeps} were a function of the flowing fracture aperture ($2b_f$), fracture width (w_f) as in PA-91 (Eqs. (12) and (13)), but unlike PA-91, weeps of various sizes ($2b_f$ and w_f) were sampled in each realization ℓ of PA-93.

To estimate the fraction of packages with seepage (f^{WPdrip}_{ECM}) and the corresponding seepage for the ECM formulation, the same analytic functions used for PA-91 were again used for PA-93 (except for the substitution of $\bar{q}^{eff}$ of Eq. (16) for $\bar{q}^{perc}$ in Eqs. (8)–(13)). As in PA-91, q^{thres} (the threshold percolation when water moves through the fractures and allows seepage) was set at the sampled matrix hydraulic conductivity of the repository horizon. Because of the reduction in percolation noted in the previous section (Fig. 5), seepage into the drift for the ECM formulation was substantially reduced in PA-93.

5. UZ Modeling in PA-95

YMP conducted PA-95 to again provide guidance on characterizing the site and two options each for the heat load and package placement in the repository [7, Appendix A; 10, Table 1]. For PA-95, the package was a large, thick-walled, multi-layer container placed in the drift. PA-95 used the Repository Integration Program (RIP) stochastic simulator to evaluate, at a 5-km boundary, (a) cumulative release at 10^4 years (Eq. (9)), and (b) individual dose over 10^4, 10^5, and 10^6 years [3, Table 4; 16; 41]. Based on previous PAs, only the release and dose for undisturbed scenario $\mathcal{A}_U$ was evaluated.

$$\bar{D}^{95}_{U}(t) = \frac{1}{n^{LHS}_{U}} \sum_{\ell=1}^{n^{LHS}_{U}=100} \sum_{r=1}^{n^{r}_{U}=39} \frac{f^{BDCF}_{U,r,\ell}}{Q^{indv}_{95,\ell}} \mathcal{R}_{U,r}(t;\mathbf{e}^{e}_{\ell})\Big|_{x^{ae}=5\text{ km}} \tag{17}$$

5.1. Climate change and infiltration in PA-95

Similar to the approach in PA–EA, two alternative distributions (i.e., alternative conceptual models or *acm*) of net infiltration (q^{infil}_{acm}) (percolation just below the evapotranspiration zone) for current arid climate conditions were used for UZ flow; however the infiltrations were a factor of 10 lower in both ranges (Fig. 5): (a) low net initial infiltration ($q^{infil}_{\text{arid,low}}(0)$ where $acm \sim low$) with a range between 0.01 and 0.05 mm/yr, uniformly distributed, and (b) high initial infiltration ($q^{infil}_{\text{arid,high}}(0)$) with a range between 0.5 and 2 mm/yr, uniformly distributed. The low net infiltration range was based on an uncertain factor of ~2 about an infiltration of 0.02 mm/yr, which had been estimated from preliminary infiltration rates observed directly over the repository [16, Figs. 2.6-2, Section 7; 42]. The high net infiltration range was based on an

[4] As explained in companion papers [5,8], YMP has considered various thermal loadings. By PA–SR and PA–LA, the repository design closely packed the packages to heat the drift above boiling but spaced the drifts 81 m apart to keep the center of the pillars below boiling in order to allow water to drain through the repository and, thereby, prevent the diversion of water to the cooler portions of the repository.

uncertainty factor of 2 about an infiltration of 1.25 mm/year, which had been estimated from the average of all preliminary infiltration rates observed in the area (excluding a high value of 13.4 mm/yr).

The influence of climate change on infiltration was modeled as a triangular wave function between current climate conditions ($q^{infil}_{\mathrm{arid,acm}}(0)$) and glacial conditions ($q^{infil}_{\mathrm{glacial,acm}}$) (Fig. 5). The period of arid conditions was sampled uniformly between 0 and 10^5 years and the cyclic period was fixed at 10^5 years similar to PA-93 ($\Delta\tau_{glacial}+\Delta\tau_{arid}=10^5$ years). The amplitude of the infiltration function was the product of the sampled initial current infiltration from either the low or high infiltration conceptual model ($q^{infil}_{\mathrm{arid,acm}}(0)$) and a uniformly distributed factor ($f^{climate}$) between 0 and 4. The latter parameter was important in PA-95 [10, Table 2]. Hence, during the time segment when net infiltration was linearly increasing from $q^{infil}_{\mathrm{arid,acm}}(0)$ to $q^{infil}_{\mathrm{glacial,acm}}$ [16, section 7.7]

$$q^{infil}_{acm}(t)=q^{infil}_{\mathrm{arid,acm}}(0)[(1+f^{climate})(t/\Delta T_{arid})] \text{ for } t\le\Delta T_{arid} \tag{18}$$

5.2. Modeled percolation in PA-95

To improve modeling of the unsaturated flow for PA-95, percolation (q^{perc}) in the UZ from the surface to the water table under ambient conditions (i.e., isothermal) was simulated based on a 1-D TOUGH2 model using the ECM formulation. The 1-D stratigraphy was a simplification of stratigraphic Column 153 of the 3-D, 30-km^2 site-scale model (UZ-94) with $\sim 10^3$ grid blocks, under development since 1992 by USGS and Lawrence Berkeley National Laboratory (LBNL) [16, Fig. ES 5-2; 43]. The top surface boundary was set at constant air pressure and precluded any water vapor movement into or out of the top surface. The bottom water table boundary was fixed at constant pressure. The mean percolation was set at the infiltration (i.e., $\overline{q}^{perc}_{ECM}(t)=q^{infil}_{ECM}(t)$).

Percolation below the repository (for use by the UZ transport module described elsewhere $\mathcal{M}^{UZtrans}$ [26]) was simplified into a matrix and fracture component. For development of this UZ flow abstraction, uncertainty in the hydrologic properties of the 1-D column below the repository was estimated by developing 10 columns (4 of which were only used for the larger but cooler repository) with randomly selected hydrologic properties from PA-93 (Fig. 8). Also for development of the UZ flow abstraction, two different assumptions as to when fracture flow initiated in the ECM formulation were simulated: fracture flow when the matrix was (a) fully saturated and (b) 95% saturated.

Uncertainty from infiltration was simulated using six fixed infiltration values in the process models. The six values were the endpoints of high and low infiltration distributions and the distribution mean (i.e., 0.01, 0.02, 0.05, 0.5, 1.0, and 2.0 mm/year)

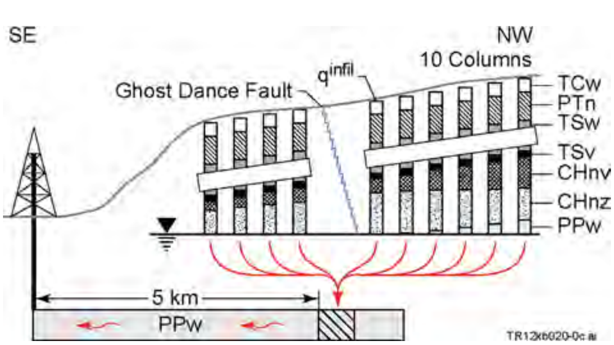

Fig. 8. For PA-95, UZ flow was evaluated in up to 10 columns with up to 7 layers that started at the surface [16, Fig. 3.8-4].

(Fig. 5). Hence, 120 simulations were conducted to represent the range of percolation behavior (10 stratigraphic columns below the repository, 2 assumptions for initiation of fracture flow, and 6 infiltration fluxes). From the 120 simulations, response functions of minimum and maximum matrix pore velocity ($v_m=q^{perc}/\phi_m s^{sat}_m=\hbar^{vel}\{q^{infil}\}$) and fraction of fracture flow f_f in 4 layers (L) below the repository ($L\sim$TSw, TSv, CHnv, and CHnz) were developed for use in the UZ transport calculations (i.e., ${}^{min}v_{m,L}=\hbar^{vel}_{\mathrm{min},L}\{q^{infil}\}$, ${}^{max}v_{m,L}=\hbar^{vel}_{\mathrm{max},L}\{q^{infil}\}$, ${}^{min}f_{f,L}=\hbar^{frac}_{\mathrm{min},L}\{q^{infil}\}$, and ${}^{max}f_{f,L}=\hbar^{frac}_{\mathrm{max},L}\{q^{infil}\}$) [16, Figs. 7.2-8–7.2-11].

During a PA-95 simulation f^{waste}_{VE} (with either the low or high infiltration alternative conceptual model) the percolation (equal to infiltration) at time t ($q^{infil}_{\mathrm{acm},\ell}(t)$), determined the minimum and maximum fracture flux fracture $f_{f,L}$ and matrix pore velocity $v_{m,L}$; for example, for matrix pore velocity,

$$v_{m,L,\ell}=\hbar^{vel}_{\mathrm{min},L}\{q^{infil}_{acm,\ell}(t)\}+U^{vel}_{\ell}[0,1]\,(\hbar^{vel}_{\mathrm{max},L}\{q^{infil}_{acm,\ell}(t)\}-\hbar^{vel}_{\mathrm{min},L}\{q^{infil}_{acm,\ell}(t)\}) \tag{19}$$

The same randomly selected index U^{vel}_{ℓ} [0,1] was used throughout the simulation ℓ at each time step. Matrix velocity in the CHnv layer (Figs. 3 and 8) would be important in PA-95 [10, Table 2].

In summary, a common abstraction approach used for various phenomena in PA-95 and later PAs consisted of (a) varying numerous parameters of a process model; (b) developing a response surface for the minimum behavior and a response surface for maximum behavior, as a function of the few parameters available during the PA simulation; and (c) then randomly sampling an index value during the PA simulation to select a value between the minimum and maximum response surfaces at each time step.

5.3. Estimated seepage in PA-95

As in PA-91 and PA-93, seepage into the drift (q^{seep}) was assumed to occur because of spatial variability of percolation relative to the permeability of the tuff at the repository horizon [16, Section 7]. In the analytic precursor to $\mathcal{M}^{Seep}$, seepage into the drift occurred whenever the spatially varying percolation at a point was greater than the hydraulic conductivity of the tuff at the repository horizon (i.e., $q^{seep}(t)=q^{seep}_{ECM,\ell}(t)-K^{TSw}$ when >0 and where K^{TSw} was log normally distributed based on information for K^{TSw} collected for PA-93 and $q^{seep}_{ECM,\ell}(t)$ had the same meaning as Eq. (8)). However, because of limitations of RIP at the time, the PA simulation could not evaluate $q^{seep}_{ECM,\ell}(t)-K_{TSw}$ for each realization ℓ and time step; hence, a response function of seepage flux (i.e., $q^{seep}=\hbar(q^{infil})$) was developed by randomly sampling the distribution of K_{TSw} and the distribution of $q^{percvar}$ to indirectly incorporate spatial variability. The corresponding response function for the fraction of packages with seepage (i.e., $f^{WPdrip}=\hbar(q^{infil})$) was estimated from the binominal distribution with a probability equal to the fraction of times that $q^{seep}_{ECM,\ell}(t)-K_{TSw}>0$ in the random samples.

During a PA-95 simulation, the infiltration ($\overline{q}^{infil}_{\ell}(t)$), as determined from Eq. (18), was used to set a range. Then a value for $q^{seep}_{\ell}(t)$ and f^{WPdrip}_{ℓ} for realization ℓ was randomly selected from the range (similar to the method described in the previous section for fracture and matrix velocity, e.g., Eq. (19)):

$$q^{seep}_{\ell}(t)=\hbar^{seep}_{\mathrm{min}}\{\overline{q}^{infil}_{\ell}(t)\}+U^{seep}_{\ell}[0,1](\hbar^{seep}_{\mathrm{max}}\{\overline{q}^{infil}_{\ell}(t)\}-\hbar^{seep}_{\mathrm{min}}\{\overline{q}^{infil}_{\ell}(t)\}) \tag{20}$$

$$f^{WPdrip}_{z,\ell}(t)=\hbar^{WPdrip}_{\mathrm{min}}\{\overline{q}^{infil}_{\ell}(t)\}+U^{seep}_{\ell}[0,1](\hbar^{WPdrip}_{\mathrm{max}}\{\overline{q}^{infil}_{\ell}(t)\}-\hbar^{WPdrip}_{\mathrm{min}}\{\overline{q}^{infil}_{\ell}(t)\}) \tag{21}$$

where $U_{\ell}^{seep}[0,1]$ was a sampled random number in realization l that represented uncertainty in the seepage. The same random number was used to evaluate both $q_{z,\ell}^{seep}(t)$ and $f_{z,\ell}^{WPdrip}(t)$. Although not considered in PA-95, flow focusing would again be considered in later PAs.

6. UZ Modeling in PA–VA

PA–VA was conducted to demonstrate the viability of the YM disposal system to Congress [7, Appendix A; 10, Table 1]. YMP used the most current information as interpreted by expert panels [17]. The emphasis was on the undisturbed release scenario class solely via a groundwater pathway, however, an early WP failure scenario was included with the undisturbed scenario ($\mathcal{A}_{U+EF}$). A gaseous pathway for ^{14}C (and possibly $^{36}Cl_2$ and $^{129}I_2$) was not included because of the anticipated change to a dose standard at a point far from the repository such that gaseous doses were inconsequential. For PA-VA, some form of all 11 modeling modules that would be used for PA-LA were present (Fig. 2).

6.1. Climate change and infiltration in PA–VA

PA–VA evaluated the influence of changes in climate over 10^6 years to precipitation, water table rise, and SZ flux using three climate states ($w(t)$) rather than the two states used in PA–EA, PA-93, and PA-95: (a) a short, arid, current climate state; (b) long-term, semi-arid climate state; and (c) short, superpluvial climate state (i.e., $w \sim arid, LTA, SP$). The short arid and superpluvial climate periods were assumed to last between 0 and 20,000 years (ΔT_{arid} uniformly distributed) except for the *present* arid climate period which was assumed to continue for between 0 and 10,000 years. The duration of the semi-arid, long-term average state was between 80,000 and 100,000 years (ΔT_{LTA} uniformly distributed). Arid and semi-arid conditions alternated back and forth until 250,000 years had passed at which time a superpluvial climate replaced the last part of the long-term average for its duration (ΔT_{SP}) sampled between 0 and 20,000 years (Fig. 5).

Rather than apply the climate changes as a percolation boundary condition for UZ flow as done in previous PAs, climates changes were applied as a precipitation boundary condition in a new infiltration module ($\mathcal{M}_{INFIL}^{Infil}$) (Fig. 9a), based on INFIL v1.0 developed by USGS, which, in turn, provided a net infiltration boundary condition to the 3-D UZ flow module, $\mathcal{M}_{TOUGH2}^{UZflow}$. Although only steady-state percolation (q^{perc}) was ultimately desired and, thus, not a function of the daily fluctuation of infiltration ($q^{infil}(t)$, the timing of precipitation and evapotranspiration had a strong influence on amount of infiltration versus runoff. To elaborate, although the average annual potential evapotranspiration is six times greater than the average annual precipitation, daily precipitation is occasionally greater than daily evapotranspiration, especially in the winter [44, Section 6.1.4].

Since infiltration was an issue of concern with the State of Nevada [45], a few more details are provided below. INFIL solved for the runoff using a daily water balance for the surface and root zone [30, Section 2.4.2; 46]

$$Q_w^{out}/A_{cell} = Q_w^{in}/A_{cell} + [q_w^{precip} - q_w^{snow} + q^{melt}] - \Delta\theta^{soil} - q^{\rm infil} - q^{ET} \quad (22)$$

where the parameters ($\mathbf{e}^e$) and temporal/spatial variables (t,$\mathbf{x}$) for the terms have been omitted for clarity. In Eq. (22), Q^{out}/A_{cell} is the surface runoff from the cell at time t and cell location $\mathbf{x}$; Q^{in}/A_{cell} is the surface run-on to the cell; q_w^{precip} is the average daily precipitation at cell location x,y adjusted for surface elevation z for the climate state w; q^{snow} is precipitation deposited as snowpack when the temperature ≤0 °C and where temperature is modeled as a sinusoidal yearly variation; q^{melt} is snow melt based on a simple empirical parameter when $T(z) > 0$ °C; $\Delta\theta^{soil}$ is the soil moisture profile requiring parameters such as soil depth, soil hydraulic conductivity, soil field capacity, soil moisture content, wilting point, and holding capacity estimated for 10 soil type groups g^{soil} developed from 40 soil classifications represented at Yucca Mountain; $q^{infil}(t,\mathbf{x};\mathbf{e}^{infil})$ is net infiltration (or percolation below the root zone) and calculated from the hydraulic conductivity K of 38 bedrock types (i.e., $\mathbf{e}^{infil} = \{K_{TCw},\ldots\}$); and q^{ET} is the evapotranspiration over a day and evaluated by adjusting a reference evapotranspiration $q_0^{ET_0}$, as calculated by the modified Priestley–Taylor equation [47, Section 4.2.6], to site specific conditions (such as surface slope and surface aspect).

The infiltration $q^{infil}(t,\mathbf{x};\mathbf{e}^{infil})$ was equal to the bedrock K when the water content of the soil layer above the bedrock exceeded field capacity [1, Section 2.3.1.3.3.1]. Generally, more infiltration occurred where the bedrock was exposed on slopes and the ridge top. In ravines and valleys, the soil cover (alluvium) trapped precipitation and runoff (for most storms) in the pores where it was drawn back out to the atmosphere through evaporation or plant transpiration.[5] The bedrock location was as determined by USGS maps [23; 30, Section 2.4.2]. The INFIL model domain extended beyond the boundaries of Yucca Mountain and the UZ-97 flow model domain. The modeled area was 228 km^2 (11 km by 20.7 km) and consisted of 254,000 nodes (30 × 30-m grid).

The infiltration model for current climatic conditions was qualitatively calibrated by varying evapotranspiration parameters $\mathbf{e}^{ET}$. Using the parameters selected, calculated water-content profiles roughly matched a few neutron-measured profiles from the 99 shallow boreholes at Yucca Mountain [6]. Infiltration maps for the two other climate states w were created using the calibrated evapotranspiration parameters.

To account for uncertainty of $q_{w,a}^{infil}(t)$, a low infiltration map and a high infiltration map were also created by respectively dividing and multiplying infiltration by 3 (i.e., $a \sim$ *base, low, high*). The factor of 3 for the high infiltration map was the maximum factor that could be used and still match observed thermal gradients at Yucca Mountain. The factor of one-third for the low infiltration map was selected to maintain symmetry [17, Section 3]. To propagate the infiltration uncertainty through the UZ flow analysis, the probability of the base precipitation and corresponding infiltration map was set at 0.6 for all climate states (i.e., $\wp\{q_{w,low}^{infil}(t)\} = 0.6$ for $w \sim arid, LTA, SP$). The probability of the low and high infiltration maps were set at 0.1 and 0.3, respectively [17, vol. 3 Table 3-5].

As input to the steady-state UZ flow calculation, a 100-yr time averaged infiltration map was determined

$$\overline{q}_{w,a}^{infil}(\mathbf{x}) = \frac{1}{\mathfrak{T}} \int_0^{\mathfrak{T}=100yr} q_{w,a}^{infil}(t,\mathbf{x};\mathbf{e}^{infil}) dt \quad (23)$$

where the infiltration $q_{w,a}^{infil}(t,\mathbf{x})$ was determined from solving Eq. (22) (i.e., the UZ flow module used a mean percolation temporally averaged over the aleatory uncertainty of precipitation and evapotranspiration timing). A total of 9 average infiltration maps: three for each climate state with each climate state having a base, low, and high value of the precipitation range (i.e., $\overline{q}_{w,a}^{infil}(\mathbf{x})$ where $w \sim arid$, LTA, and SP and $a \sim$ *base, low, high*) [17, vol. 3 Section 3.1.1.1, Table 3-5] (Fig. 10a).

[5] The ability of thick alluvium to prevent deep vertical water movement in a desert environment was an important advantage mentioned by USGS when suggesting a repository in the Basin and Range providence, in general, and the Nevada Test Site (NTS), in particular [48,49]. This behavior of alluvium was an important phenomenological barrier of the Greater Confinement Disposal (GCD) facility, which disposed of classified transuranic (TRU) waste and low-level waste (LLW) in 36-m deep boreholes in a 900-m thick layer of tuff alluvium at NTS [50].

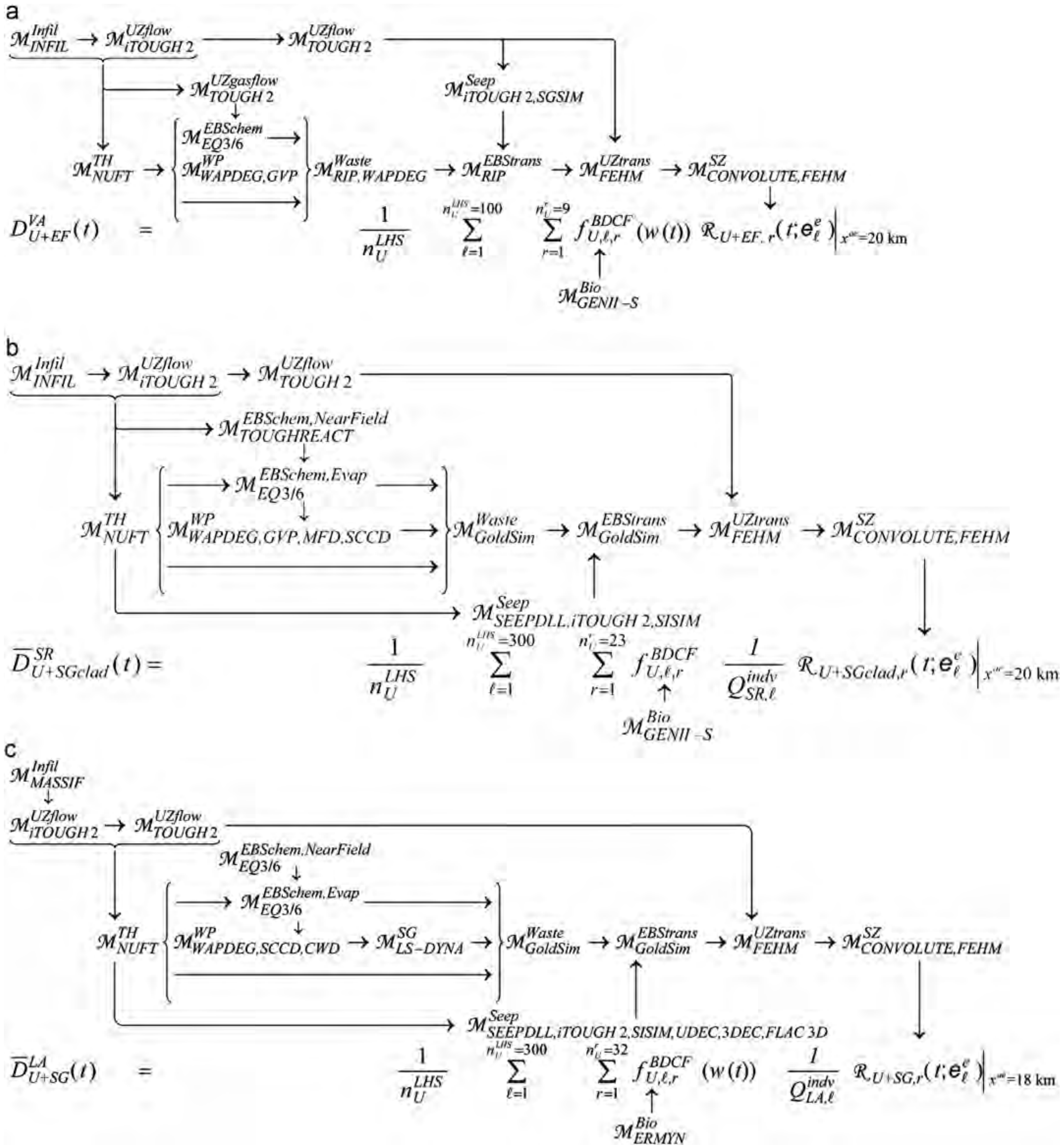

Fig. 9. Linkage of modules for major PAs for YM repository [7] (a) PA–VA, (b) PA–SR, and (c) PA–LA.

The average infiltration at the surface over the ~3.0 km^2 repository area was greater for current conditions and substantially greater for future climates than used in PA-95 [17, vol. 3 Section 3.1.1.1]: 7.7 mm/yr for the base for current, arid climate ($\overline{q}^{infil}_{arid,base}$) when using the full set of infiltration observations available for PA–VA [6] versus 1.25 mm/yr (when using the few preliminary data available for PA-95); 42 mm/yr median for long-term, semi-arid climate ($\overline{q}^{infil}_{LTA,base}$); and 110 mm/yr median for superpluvial climate ($\overline{q}^{infil}_{\mathrm{SP,base}}$). Earlier PAs, such as PA-EA and PA-93 had considered high infiltration but only up to 20 and 70 mm/yr, respectively (Fig. 5).

6.2. Percolation in PA–VA

Generally, percolation was thought vertical above the repository except for some lateral diversion along stratigraphic unit boundaries where fracture and matrix properties change abruptly. However, substantial lateral flow below the repository in areas where perched

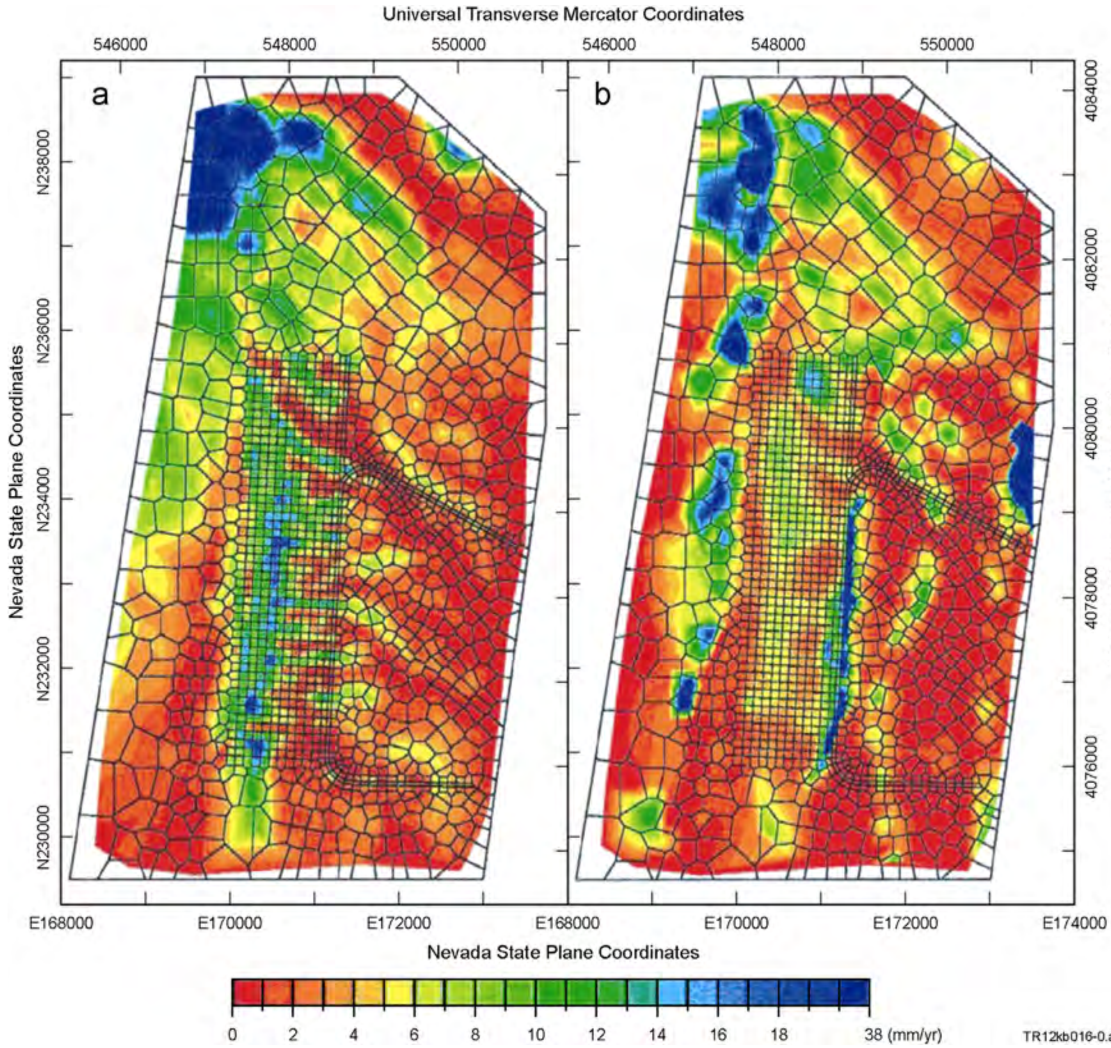

Fig. 10. UZ flow in PA–VA for base case (60% of simulations) at current, arid conditions [51, Figs. 3 and 13]: (a) net infiltration at surface (7.7 mm/yr over repository area and 4.9 mm/yr over UZ model domain [30, p. 2–28]), and (b) percolation (matrix and fracture flux) at repository level.

water exists was thought to occur at the time of the PA–VA and thereafter [17, vol. 3 Figs. 3–8; 30, Figs. 2-95, 2-96, 2-102].[6] Perched water was observed above the low-permeability units represented by the basal vitrophyre of the Topopah Spring welded (TSw3) and the northern portion of the nonwelded, tuff of the Calico Hills (CHn1) that was zeolithic. Thus, a 3-D mountain-scale model (UZ-97) was built for PA–VA to evaluate percolation flow fields for the UZ flow module ($\mathcal{M}^{SZflow}$) [51,52], based on the multiphase code, TOUGH2, developed by LBNL [53] (Fig. 9a). The UZ-97 process model included 24 homogeneous hydrologic units and had a 100-fold increase in spatial resolution from the UZ-94 process model (3.9×10^4 grid blocks in UZ-97 model covering 5×9 km—~43 km^2—and 0.8 km deep to water table) [6; 17 vol. 3 Section 3; [51; 52].

Similar to PA-95, the UZ-97 mountain-scale model used the option in TOUGH2 based on Richard's Equation and isothermal conditions and, thus, movement of air or water vapor from thermal gradients was not modeled in $\mathcal{M}^{UZflow}$. However, air and water vapor movement was modeled in the thermal module ($\mathcal{M}^{TH}$) used for container degradation and described elsewhere [8]. The UZ-97 process model (and all those following) used the new dual-permeability model (DKM) option in TOUGH2 that modeled fractures and matrix as distinct continua that could be in disequilibrium with each other but would interact through a mass transfer term ($\dot{m}_f$) at every point within the model domain. Hence, two continuum equations—fracture and matrix—were solved at each of the 3.9×10^4 grid blocks rather than one as for the ECM used in earlier PAs (Eq. (3)). Also, TOUGH2 solved the integral form of the system of partial differential equations[7]

$$\partial \int \rho^w s_f \phi_f / \partial t = \int \nabla \bullet \frac{\rho^w \mathbf{k}_f k_f^{rel}}{\mu^w} \nabla (P_f + \rho^w g z) dV + \int \dot{m}_f dV \tag{24}$$

$$\partial \int \rho^w s_m \phi_m / \partial t = \int \nabla \bullet \frac{\rho^w \mathbf{k}_m k_m^{rel}}{\mu^w} \nabla (P_m + \rho^w g z) dV - \int \dot{m}_f dV \tag{25}$$

where ρ^w is the liquid density, s_Ω is saturation for either the matrix or fracture domain ($\Omega \sim m,f$), ϕ_Ω is the media porosity (and where

[6] Percolation below the repository had been noticeably diverted down dip to faults east of the repository footprint in the 3-D USGS/LBNL process model (UZ-94) in 1995 but was not incorporated into a PA until PA–VA.

[7] Because TOUGH2 was not formulated to calculate steady state conditions directly (i.e., $\partial \int \rho^w s_\Omega \phi_\Omega / \partial t$ set to zero), millions of years had to be simulated before an asymptotic steady-state solution was reached [54, Section 6.2.4]. The simulation length indicates how difficult the numeric calculations were because of the orders

$\phi_\Omega s_\Omega = \theta_\Omega$ or the volumetric moisture content), μ^w is the liquid viscosity, $\mathbf{k}_\Omega$ is the permeability tensor, k_Ω^{rel} is the relative permeability evaluated below (and where $\mathbf{k}_\Omega k_\Omega^{rel} \rho^w g/\mu^w = \mathbf{K}$ or hydraulic conductivity), g is the gravitational constant, P_Ω is the liquid pressure, z is the vertical coordinate distance, and where the dependence on location $\mathbf{x}$ is understood and omitted for clarity. The $\dot{m}_f$ is the mass flow rate between fractures and the tuff matrix and assigned as

$$\dot{m}_f = \begin{cases} -(s_m^{eff})\dot{m}_f^{eff} & \text{if } P_m^{cap} \geq P_f^{cap} \\ -\dot{m}_f^{eff} & \text{otherwise} \end{cases} \tag{26}$$

$$\dot{m}_f^{eff} = \frac{k_f k_f^{rel}}{\mu} \rho_w (P_f^{cap} - P_m^{cap}) \frac{a_f^{shape}}{2B_f + 2b_f} A^{fm} \tag{27}$$

where $2B_f$+$2b_f$ is the fracture spacing, a_f^{shape} is a fracture shape factor and equal to 6 for parallel, infinite fractures uniformly space, and A^{fm} is the fracture-matrix interface area. For PA–VA, the fracture-matrix area A^{fm} was the geometrical fracture-matrix area reduced by the fracture saturation s_f^{sat} in the nonwelded tuff units and by a constant reduction factor of 0.0005 in the welded tuff units [52]. The van Genuchten formulation (Eqs. (4)–(7)) was used for evaluating the relative permeability and capillary pressure of Eq. (27).

An inversion model (based on the LBNL iTOUGH2 v2.2) [56] was used to calibrate the hydrologic properties (Fig. 9a). However, a 3-D inversion for all parameters and all layers was not possible with a reasonable amount of time for PA–VA and thereafter. Hence, only 1-D inversion was performed for several columns and groupings of layers [6,57,58]. Furthermore, a reduced parameter set was calibrated as follows [6].

The parameter $\alpha_f^{van}(\mathbf{x})$ of the van Genuchten formulation quantifies the capillary pressure in a fracture (P_f^{cap}) in Eq. (27) and is proportional to the fracture aperture ($2b_f$). The $\alpha_f^{van}(\mathbf{x})$ was constrained to 3 relative values (low, base, or high) for each of the homogeneous model layers. Although more were created for sensitivity studies, only 3 of the 9 possible combinations of the 3 relative values of $\alpha_{f,a}^{van}$ (where *a*∼*low, base, high*) with the three infiltration maps at the current arid climate ($q_{arid,a}^{\text{infil}}(\mathbf{x})$) were developed for PA–VA to produce 3 infiltration-hydrologic property sets *h*∼*base, low, high*) (i.e., base $\alpha_{f,base}^{van}$values were combined with the base infiltration map, low $\alpha_{f,low}^{van}$ values were combined with the low infiltration map, and high $\alpha_{f,high}^{van}$ values were combined with the high infiltration map) [59, Section 11.2.1.3].[8] The final step was to manually calibrate a 3-D model to produce perched water at known well locations [6] and evaluate consistency with geochemical modeling [6,60].

The 3 calibrated infiltration-hydrologic property sets *h* were used to calculate steady-state percolation flow fields for all three climate states using the time averaged infiltration (Eq. (23)). Thus, 9 steady-state percolation flow fields $q_{w,h}^{perc}(\mathbf{x})$ were calculated (i.e., product of 3 calibrated infiltration-hydrologic property sets *h*∼*base, low, high* and 3 climate states *w*∼*arid, LTA, SP*). The calibrated infiltration-hydrologic property sets were also used for the seepage and thermal-hydrologic models (Fig. 9a) [17, vol. 3, Figs. 2–13]. The spatially averaged percolation at the repository level was ∼5.5 mm/year versus the ∼6.7 mm/year at the surface (18% reduction) and shifted flow laterally ∼500 m to the east (Fig. 10b) [51, p. 210].

The spatially varying percolation was grouped into 6 zones *z* for use in evaluating seepage, WP degradation, and waste form degradation (i.e., $\overline{q}_{z,w,h,\ell}^{perc}$ replaced $q_{w,h,\ell}^{perc}(\mathbf{x})$ for use in $\mathcal{M}^{Seep}$, $\mathcal{M}^{WP}$, $\mathcal{M}^{waste}$). Precipitation zones were also used for PA–LA but precipitation bins were used for PA–SR. Furthermore, the module where this grouping step was conducted would change to $\mathcal{M}^{TH}$ after PA–VA.

During a PA–VA simulation, the analysis would instantaneously switch between $q_{arid,h}^{perc}$,$q_{LTA,h}^{perc}$, and $q_{SP,h}^{perc}$ at the sampled time that the climate changed occurred. Hence, the time dependence of percolation was developed from linking the 3 steady-state values; for example,

$$q_{z,\ell}^{perc}(t) = \begin{cases} q_{arid,low}^{perc} & \text{if } t < \Delta\tau_\ell^{arid} \\ q_{LTA,low}^{perc} & \text{if } \Delta\tau_\ell^{arid} \leq t < \Delta\tau_\ell^{LTA} \text{ and so on} \end{cases} \tag{28}$$

where the sequence continues using the same *h* property at each climate state (*h*∼*low* in the above example). Percolation will often be displayed as a function of time and not the climate state $w(t)$ in the remainder of the text.

6.3. Seepage into drift in PA–VA

In PA–VA as in past PAs, seepage in the drift was expressed as a probability distribution of the spatially uncertain seepage flow rate (Q^{seep}) and a probability distribution of the spatially uncertain fraction of packages contacted (f^{WPdrip}), both as a function of percolation flux (q^{perc}) [17, vol. 3, Fig. 3–13]. However for PA–VA, seepage distributions were developed from a new seepage module $\mathcal{M}^{Seep}$ (Figs. 2 and 9b).

In $\mathcal{M}^{Seep}$, the distributions for f^{WPdrip} and Q^{seep} were developed by parametrically varying parameters of a 3-D seepage model for PA (SMPA) of a single drift with 5-m diameter opening to represent the disposal drift. SMPA was a detailed process model of diversion of percolation around a disposal drift, which acts as a capillary barrier to percolating water near the drift [61,62]. The model was of a drift segment 20-m high, 15-m wide, and 45-m long that used 0.5-m cube grid blocks. SMPA, based on TOUGH2, only represented the fracture continuum. Seepage occurred predominantly from flow in the fractures because matrix permeability was so low [17, vol. 3, Section 3.1.1.4; 30, Section 2.4.4.10].

The sequential indicator code SGSIM [63, p. 1411–2] was used to generate 3 geostatistical variations of k_f about 3 mean $\overline{k}_f$ values. Air permeability measurements, based on air injection tests conducted in preparation for the Drift Scale Test (DST) to evaluate thermal effects [6], were used to select those $k_f(\mathbf{x})$ fields that produced results which reasonably matched the air injection measurements (i.e., the analyst manually conditioned the generated $k_f(\mathbf{x})$ fields).

A total of 108 cases were run with SMPA at 4 discrete q^{perc}, 3 discrete $\overline{k}_f$, and 3 α_f^{van} (where the values for $\overline{k}_f$ and α_f^{van} spanned the range of the 3 repository layers Tptpmn, Tptpll, Tptpln of Fig. 2), and 3 geostatistical variations of k_f about the mean $\overline{k}_f$. The uncertainty in the 2 parameters $\overline{k}_f$ and α_f^{van} was selected based on preliminary sensitivity analysis [17, Table 3-7; 30, Section 2.4.4.10].

The 108 results were used to define a mean and standard deviation for Q^{seep} and f^{WPdrip} as a function of q^{perc}; that is [17, vol. 3, Table 3-7; 30, Section 2.5.2.4],

$$\overline{Q}^{seep} = \hbar(q^{perc}),\ \sigma^{Q^{seep}} = \hbar(q^{perc}),\ \overline{f}^{WPdrip} = \hbar(q^{perc}) \text{ and } \sigma^{f^{WPdrip}} = \hbar(q^{perc}) \tag{29}$$

(*footnote continued*)
of magnitude differences in permeability between layers, the fractures and matrix, and nonlinear two-phase flow properties.

[8] Although the details of developing the calibrated infiltration-hydrologic property sets differ for PA–SR and PA–LA, both later studies continued to produce a small number of calibrated infiltration-hydrologic property sets (3 in PA–SR and 4 in PA–LA).

Although spatial variability in k_f was considered in developing the functions, uncertainty in $\bar{k}_f$ and α_f^{van} was also included; hence, the standard deviations, $\sigma^{Q^{seep}}$ and $\sigma^{f^{WPdrip}}$ represented a mixture of uncertainty and variability. The uncertainty and spatial variability would be separated for PA–SR and PA–LA.

The mean and standard deviations were used to define 72 beta distributions, based on $\overline{Q}^{seep}(\overline{q}^{perc}_{z,w,h})$, $\sigma^{Q^{seep}}(\overline{q}^{perc}_{z,w,h})$, $\overline{f}^{WPdrip}(\overline{q}^{perc}_{z,w,h})$, and $\sigma^{f^{WPdrip}}(\overline{q}^{perc}_{z,w,h})$) along with a minimum of zero for both Q^{seep} and f^{WPdrip}, and a maximum of 10 $\sigma^{Q^{seep}}$ for Q^{seep}, and a maximum of 1 for f^{WPdrip} [30, Section 2.5.2.4]. Because the average percolation ($\overline{q}^{perc}_{z,w,h}$) in each of the 6 zones z and 9 UZ flow fields was available, the 72 beta distributions of Q^{seep} and f^{WPdrip} could be developed prior to the PA–VA stochastic simulation with RIP.

During a PA–VA simulation with RIP, the LHS realization ℓ sampled either a low (0.3 fraction of time), base (0.6 fraction of time), or high (0.1 fraction of time) calibrated infiltration-hydrologic property set h and corresponding flow field $\overline{q}^{perc}_{z,w,h,\ell}$. The appropriate subset of beta distributions were then selected and sampled (maintaining perfect correlation between the distributions) [59, Section 11.2.1]. The spatial uncertainty in f^{WPdrip} was the most important parameter influencing the uncertainty in dose in PA–VA [10, Table 2].

7. UZ flow modeling for PA–SR

In late 2000, YMP completed PA–SR to inform the decision of the Secretary of Energy and President concerning the YM site for a repository [7, Appendix A; 10, Table 1]. Hence, a more concerted effort was made to describe the underlying models of the PA. Based on past tradition in early reactor studies and in concert with the 1999 proposed 10 CFR 63, which called for the concept of reasonable assurance [3,64], the YMP made liberal use of conservatisms in model choices and parameter assignments in PA–SR.

The expected total dose included the contribution of the undisturbed scenario class plus seismic failure of cladding ($\mathcal{A}_{U+SGclad}$) and igneous dike intrusive releases ($\mathcal{A}_{VE}$, and $\mathcal{A}_{VI}$) for the first time since PA-93. Per the new EPA radiation protection standard, 40 CFR 197, the consequence of the human intrusion scenario were evaluated but its probability was not, and, thus, the expected dose was not included. The $\overline{D}^{SR}_{U+SGclad}(t)$ was calculated for $t<10^6$ years at a 20-km boundary from 23 radioisotopes r using 300 samples ℓ of the numerous epistemic parameters $\mathbf{e}^e_\ell$ (Fig. 9b)

7.1. Climate change in PA–SR

PA–SR (and PA–LA) considered two small climate changes in the first 10^4 years [18, Table 4-9]: (a) change from present arid conditions (interglacial climate) to semi-arid conditions after 600 years caused by a general monsoonal weather pattern over southern Nevada (monsoon climate), and (b) moderate semi-arid conditions after 2000 years caused by a transition to a glacial weather pattern (glacial-transition climate). Climate changes were at fixed times rather than sampled times as in PA–VA, and based on examination of the earth orbit changes in eccentricity (oscillation in the elliptical shape of earth's orbit every 10^5 years) and precession (wobble of earth's axis like a spinning top every 2.3×10^4 years) [65]. PA–SR did not consider future climate change after the 10^4 years regulatory period; but for the PA for the February 2002 final Environmental Impact Statement (EIS) for the site recommendation, the glacial-transition period after 2000 years was extended to 10^6 years (Fig. 5).[9]

The concept of $\mathcal{M}^{Infil}$ remained the same as in PA–VA, but for PA–SR, INFIL v2.0 improved the representation of evapotranspiration from the root zone q^{ET} and included surface water routing and infiltration from surface run on in channels Q_{on}/A_{cell} (Eq. (22)). Furthermore, the bedrock data used by q^{infil} and $\Delta\theta_{soil}$ respectively, were updated using new USGS information [44, Section 6.6.4]; and (2) the development of the daily precipitation q^{precip}_w was improved [6].

Similar to PA–VA, 3 levels (base, low, and high) of precipitation for the 3 climate states were used to propagate the uncertainty in infiltration, which again resulted in 9 infiltration maps. Monte Carlo analysis was used to estimate probability weights of 0.17, 0.48, and 0.35 for the base, low, and high infiltration maps, respectively [44, Section 7.2]. The average infiltration at the surface over the 4.6 km^2 repository area was less for current and future climates than used in PA–VA [44, Tables 6-10, 6-14, 6-19] and centered around the glacial and pluvial climate values used for PA-93 and PA–EA, respectively (Fig. 5). The spatial distribution of net infiltration for PA–SR was similar to PA–VA, but the absolute values were reduced (Fig. 11a).

7.2. Percolation at repository horizon in PA–SR

For PA–SR, the basic approach to estimating percolation at the repository level remained the same as in PA–VA in that both a property calibration model and a fluid-flow applied model were built. For PA–SR, however, an active fraction model was implemented into TOUGH2 and the 1-D calibration with iTOUGH2 v3.2 was more extensive.

The active fracture model (developed for YMP by LBNL) consisted of revised van Genuchten parameters for flow in the fractures. A fracture-matrix coupling parameter ($\gamma^{fm}(\mathbf{x})$), expressed as a fraction between 0 and 1 and a function of location, was defined that quantified the fraction of fracture surfaces wetted by the liquid water phase in the representation of k_f^{rel} and capillary pressure P_f^{cap} as follows [55]:

$$k_f^{rel}=(s_f^{eff})^{\frac{1+\gamma^{fm}}{2}}\left[1-\left(1-(s_f^{eff})^{\frac{1-\gamma^{fm}}{m_f^{van}}}\right)^{m_f^{van}}\right]^2 \tag{30}$$

$$P_f^{cap}=\frac{1}{\alpha_f^{van}}\left[(s_f^{eff})^{\frac{\gamma^{fm}-1}{m_f^{van}}}-1\right]^{1-m_f^{van}} \tag{31}$$

where expressions for matrix properties P_m^{cap} and k_m^{rel} are similar except with $\gamma^{fm}(\mathbf{x})$ omitted (and, thus, identical to the original van-Genuchten formulation (Eqs. (5) and (6)).

Another change for PA–SR was the addition of a step for calibrating fault properties using a 2-D model with iTOUGH2 [6,68]. As with PA–VA, the final step was the manual calibration of a 3-D mountain-scale model based on TOUGH2 v1.4 to set fracture properties to produce perched water at known well locations [69, Table V-1]. However, two conceptual models of flow near the perched water were developed. The first conceptual model was similar to PA–VA and assumed some flow through fractures at the perched zones of the northern zeolitics of the CHn, which allowed some sorption of radionuclides in the zeolites. The second conceptual model assumed no connected fractures existed through the zeolitic layer at the perched water zone (thus, no sorption occurred). Both models predicted significant lateral flow in the northern portion of the CHn1 [29, Section 3.7.3.3]. The

[9] In the initial promulgation of 40 CFR 197, EPA required the environmental impact statement (EIS) to evaluate performance over 10^6 yrs [3].

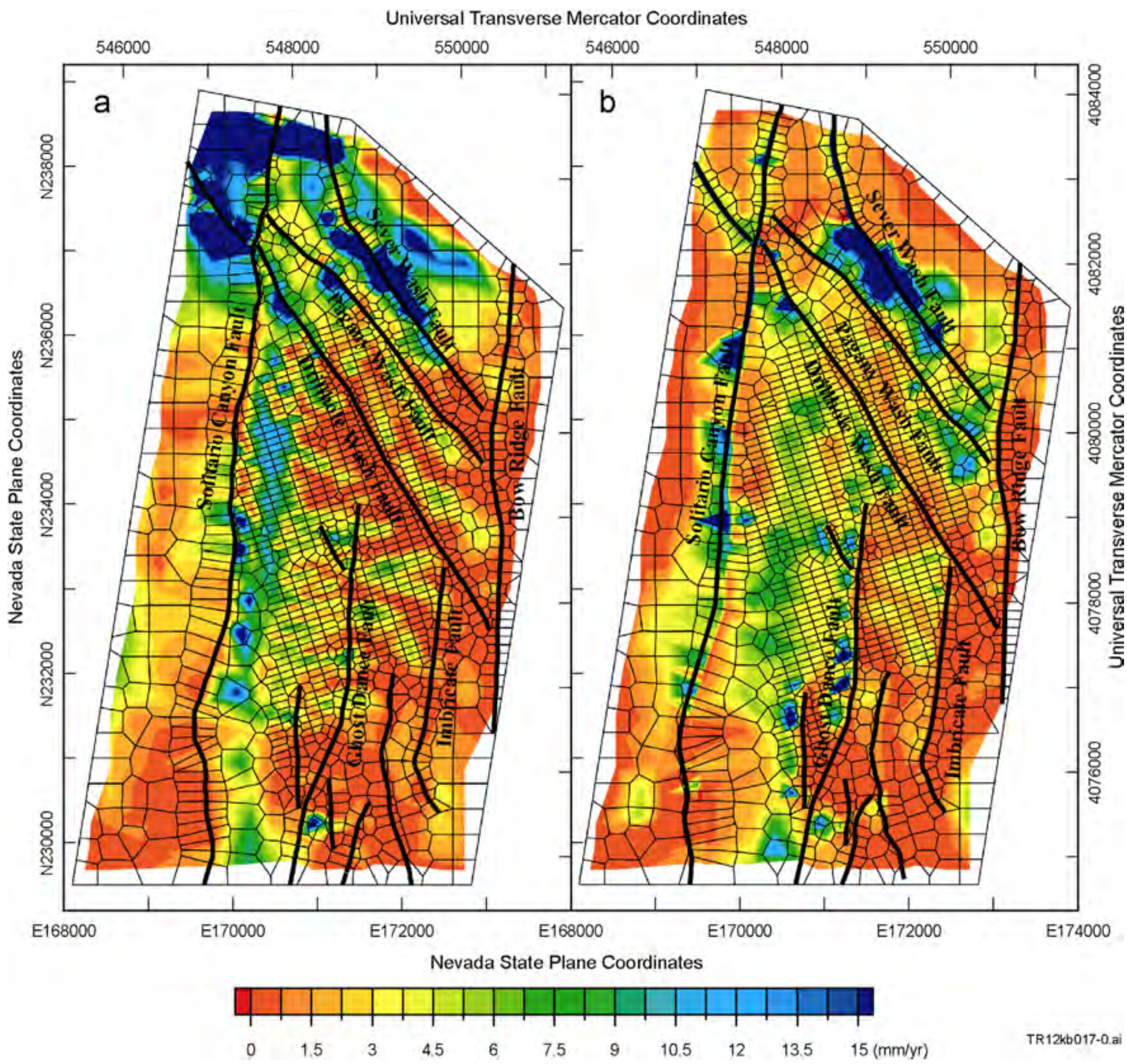

Fig. 11. UZ flow in PA–SR for base case (48% of simulations) at current, arid conditions [66; 67, Figs. 4 and 7]: (a) net infiltration at surface from INFIL v2.0 (4.1 mm/yr over repository area), and (b) percolation (matrix and fracture flux) at repository.

slightly more conservative second conceptual model was used (i.e., only 3 rather than 6 calibrated infiltration-hydrologic property sets were used). For development of thermal functions in $\mathcal{M}^{TH}$ (discussed in a companion paper [8]), the 3 calibrated infiltration-hydrologic property sets were used. For development of the seepage function in $\mathcal{M}^{Seep}$, only the base hydrologic property set was used [70, p. 3–32].

The 3-D mountain-scale flow UZ-99 process model had almost a 2-fold increase in spatial resolution from the UZ-97 process model (5.4×10^4 grid blocks in the 3D UZ-97 model [52] versus 9.8×10^4 grid blocks in the 3D UZ-99 model) [67; 69, Table VI-1] and modeled 32 hydrologic layers (30 layer properties were unique) [6] (Fig. 3). Using the UZ-99 process model, 9 flow fields were generated for the 3 infiltration-hydrologic property sets h and 3 climate states [71]. The uncertainty in calibrated infiltration-hydrologic property sets, as represented by h, was an important parameter in PA–SR [10, Table 2].

As noted for PA-91, USGS predicted the transition from a high to low porosity at the interface could cause flux to be diverted laterally down slope to the faults and away from the repository in 1984. However, the UZ flow models built between 1995 and 2000, with gradual transitions of rock properties near the PTn, did not observe noticeable diversion down slope at the PTn/TSw interface. However, for PA–SR and PA–LA, the UZ model, with greater resolution of the PTn layer, did show some diversion by the TCv/PTn layer interface to the northwest of the repository footprint [1, Section 2.3.2.4.2.1.1; 71] (Fig. 11b). To the northwest, flow was diverted down dip (i.e., eastward from the crest) to faults such that infiltration flux at the surface and percolation flux at the repository level were different [31;39, Fig. 6.3.1-7; 72]. The estimated lateral diversion over the UZ model domain for PA–SR was 4% near the surface, 15% at the PTn/TSw interface above the repository, and 35% at the interface below the repository of the low-permeability Topapah Spring vitrophyre (TSw3) and zeolitic tuff in the northern portion of Calico Hills Formation (CHn1) [18, Figs. 4-24, 4-25; 29; 54, Figs. 6-58, 6-59] (Fig. 3).

7.3. Seepage in PA–SR

The evaluation of the seepage in $\mathcal{M}^{Seep}$ for PA–SR was much more elaborate than for PA–VA. Specifically, a new 3-D seepage calibration model (SCM) was added to the seepage simulation model for PA (SMPA) [29, Sections 3.9.4, 3.9.5]. Furthermore, $\mathcal{M}^{Seep}$ separated spatial variability and epistemic uncertainty.

The purpose of SCM was again to develop calibrated properties of $k_f(\mathbf{x})$, $\phi_f(\mathbf{x})$, and $\alpha_f^{van}(\mathbf{x})$. For PA–SR, SCM modeled the geometry of the niche at Station 36+50 (Niche 3650) located near the Sundance Fault in the exploratory studies facility (ESF) where water-release and air injection measurements had been made [6, Fig. 4; 73,74] (Fig. 1). The calibrated infiltration-hydrologic property sets from the UZ mountain scale model at the base infiltration were used as a starting point ($h \sim base$). Water-release tests above Niche 3650 were used in iTOUGH2 v3.2 to adjust $\phi_f(\mathbf{x})$ and $\alpha_f^{van}(\mathbf{x})$. Heterogeneous fracture permeability fields were generated using the sequential indicator code SISIM [63, p. 141], and reasonable fields selected using the Niche 3650 air injection tests (rather than the DST air injection tests used in PA–VA) [6, Fig. 4] (Fig. 9b).

The adjusted properties were then used in SMPA. SMPA was a 15-m wide, 20-m tall section normal to the drift and 5.23 m along the drift (container length of 5.1 m plus 0.1 m spacing) using 0.5 m cube grid blocks (same as PA–VA). Similar to PA–VA, the purpose of SMPA was to develop epistemic uncertainty distributions for seepage fraction (f^{WPdrip}), mean seepage ($\overline{Q}^{seep}$), and aleatoric seepage spatial variability $\sigma^{Q^{seep}}$ as a function of percolation (q_f^{perc}) (where variability in f^{WPdrip} was not evaluated in PA–SR and thereafter). The epistemic uncertainty was determined from parametrically varying parameters in 720 simulations (versus 108 in PA–VA), which consisted of a combination of 5 values of q_f^{perc}, 4 values of $1/\alpha_f^{van}$, 4 values of $\overline{k}_f$, 3 values of the spatial variability of fracture permeability ($\sigma^{\ln(\overline{k}_f)}$), and 3 realizations of a conditioned permeability field ($k_f(\mathbf{x})$) about $\overline{k}_f$. Functions were developed to define the three points of triangular distributions of epistemic uncertainty for f^{WPdrip}, $\overline{Q}^{seep^E}$ and spatial variability as $\sigma^{Q^{seep}}$; for example, for $\overline{Q}^{seep^E}$

$$ {}^{\min}\overline{Q}^{E}_{seep} = \hbar^{\min}\{q_f^{perc}\},\quad {}^{mode}\overline{Q}^{E}_{seep} = \hbar^{mode}\{q_f^{perc}\},\ \text{and} $$
$$ {}^{\max}\overline{Q}^{E}_{seep} = \hbar^{\max}\{q_f^{perc}\} \tag{32} $$

Because PA–VA had used percolation averages $\overline{q}_{z,\ell}^{perc}(t)$ from $\mathcal{M}^{UZflow}$, PA–VA had implicitly assumed changes in percolation during the thermal period could be neglected when determining the average seepage (except to stop seepage when the drift wall temperature was > 100 °C). Furthermore PA–VA had assumed average seepage could be calculated using the average percolation, which is only true for a fairly linear relationship between seepage and percolation (i.e., $\overline{Q}_{z,l}^{seep}(q_\ell^{perc}(t,\mathbf{x})) \approx Q_{z,\ell}^{seep}(\overline{q}_{z,\ell}^{perc}(t))$. Both assumptions would be removed for PA–SR. First, percolation was set at the value at each of the 610 locations $\mathbf{x}$ from the thermal hydrologic $\mathcal{M}^{TH}$ module ($q_{b,p,h,\ell}^{perc}(t,\mathbf{x},B^{option})$. Second, epistemic samples of $\overline{Q}_{b,p,h,\ell}^{seep}(t,\mathbf{x},B^{option})$, $\sigma_{b,p,h,\ell}^{Q^{seep}}(t,\mathbf{x};B^{option})$, and $f_{b,p,h,\ell}^{WPdrip}$ from the triangular distributions (e.g., Eq. (32) for $\overline{Q}_{b,p,h,\ell}^{seep}(t,\mathbf{x},B^{option})$) were used to develop beta distributions using $q_{b,p,h,\ell}^{perc}(t,\mathbf{x},B^{option})$. The triangular distributions and, thus, the beta distributions would change with bin b, package type p, location $\mathbf{x}$, time t (i.e., change in climate state w); and backfill option B^{option}. In turn, the beta distributions were sampled to define a spatially variable seepage ($Q_{b,p,h,\ell}^{seep}(t,\mathbf{x};B^{option})$) at each of the 610 locations $\mathbf{x}$. The resulting spatially variable seepage was grouped into 3 EBS dripping environments (always, intermittent, and never dripping or $d \sim drip,inter,no\text{-}drip$) and an average seepage calculated ($\overline{Q}_{b,p,d,\ell}^{seep}(t;B^{option})$) for each bin b and drip environment d. The necessary repetitive processing to produce $Q_{b,p,h,\ell}^{seep}(t,\mathbf{x};B^{option})$and $f_{b,p,h,\ell}^{WPdrip}(t,\mathbf{x};B^{option})$ and then calculate spatial bin averages for $\mathcal{M}^{WP}$ and $\mathcal{M}^{Waste}$ at each time step of a Goldsim® simulation was performed by the newly developed SEEPDLL [7, Fig. 6; 75, p. 129] (Fig. 9b).

The secondary influence of drift degradation on seepage through a change in shape from circular to oval had not been considered in PA–VA, although elimination of drift backfill had been suggested in 1994. For PA-SR, analysis of degraded drift geometry was evaluated using the geomechanical codes UDECv2.0 and DRKBA v3.3 [7, Fig. 6] (Fig. 9b). Seepage analysis was conducted with the various shapes and the average increase in seepage was 50%; hence, a factor of 1.50 was applied to the $\overline{Q}_{b,p,d,\ell}^{seep}(t;B^{option})$results for PA–SR.

Although important for PA–VA, $f_{b,p,d,\ell}^{WPdrip}(t)$ was not important for PA–SR because (a) container corrosion no longer differentiated between dripping (wet) and non-dripping (humid) environments, and (b) advective flow through the package did not occur until late in the simulation after much corrosion.

8. UZ flow modeling for PA–LA

In July 2002, President Bush signed the *Yucca Mountain Development Resolution* authorizing DOE to apply to NRC for a license to construct the repository. An unpublished interim PA was conducted in 2004, but DOE did not proceed to submit application because the Licensing Support Network (LSN) for documents supporting the application was not certified as complete [3, Appendix B.]. Most of the major modeling changes between PA–SR and PA–LA occurred for this first interim PA, such as inclusion of the seismic disruptive scenario class.

Another unpublished interim PA was conducted in 2005, but DOE did not proceed to submit an application in order to adopt a new transportation, aging, and disposal (TAD) handling canister to facilitate operations at the site, adhere to the EPA and NRC proposed 10^6 years regulatory period, replace the infiltration model, adopt a modular design for the repository surface and subsurface [5], and continue to improve documentation. A third iteration became the basis for the SAR/LA submitted to NRC in June 2008 [1,2]. The expected total dose for the undisturbed scenario class included seismic ground motion $\overline{D}_{U+SG}(t)$ calculated for $t < 10^6$ years (Fig. 9c).

8.1. Climate change and infiltration in PA–LA

PA–LA simulated conditions to 10^6 years to estimate $q^{infil}(t,\mathbf{x};\mathbf{e}^{infil})$. For the first 10^4 years, PA–LA was based on the same future climate analysis as PA–SR: thus, the same time of climate changes (600 and 2000 years) and the same analog sites were selected for estimating precipitation and temperature in future states [18, Table 4-9] (Fig. 4). As requested by EPA [76], NRC defined the modeling style for climate change after 10^4 years in the 2005 draft revision of 10 CFR 63 [32]. NRC proposed DOE use an overall average percolation rate at the *repository* horizon that was to be held constant for the post 10^4 years period as sampled from a loguniform distribution between 13 and 64 mm/yr (i.e., 5% to 20% of estimated 266–321 mm/yr of precipitation at surface) (Figs. 4 and 5). YMP estimated the net infiltration ranges at the surface that would produce the average percolation at the repository level specified by NRC such that spatially varying percolation was present in the analysis, which was consistent with the spatially varying percolation observed for the earlier climate states.[10]

In October 2005, DOE directed SNL to repeat implementation of the infiltration model [6,77]. As more fully described in a companion paper [6], this reevaluation occurred because the YMP discovered correspondence between USGS geohydrologists in November 2004 that raised questions about fabrication of QA records (such as when computer programs related to INFIL were installed). SNL developed the code MASSIF, which used the same underlying concepts based on mass balance, as INFIL (Eq. (22)) [1, Section 2.3.1.3.3.1.1; 44], Section

[10] In March 2009, NRC promulgated changes to 10 CFR 63 that revised the distribution of percolation to consider at the repository level, based on more background analysis: lognormal distribution truncated between 10 and 100 mm/yr. The extension of the distribution to 100 mm/yr required producing a new UZ flow field but caused only subtle changes to the PA–LA results.

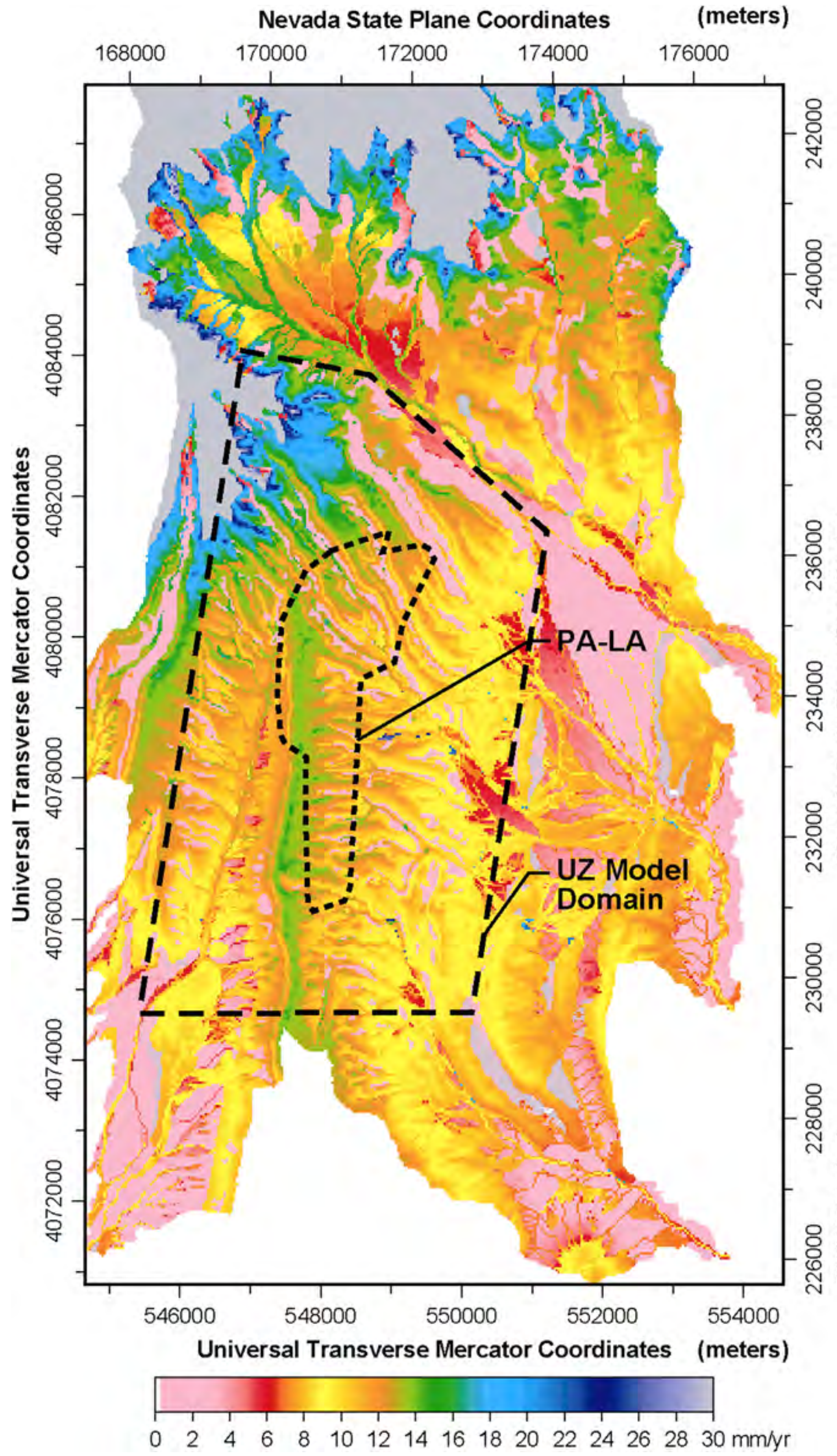

Fig. 12. Median net infiltration for PA–LA from MASSIF (14 mm/yr over repository area).

6.4.4]. However, MASSIF (1) added uncertainty in soil depth and uncertainty in bedrock permeability for two of 38 bedrock types to evaluate the soil moisture profile $\Delta\theta^{soil}$ [1, Section 2.3.1.3.2.1.3]; (2) improved development of the synthetic q^{precip}; (3) evaluated evapotranspiration q^{ET} using international guidelines on estimating coefficients [1, Eq. (2.3.1-7)]; (4) evaluated the reference evapotranspiration (q_0^{ET}) with the more complete Penman–Monteith equation, rather than the Priestley–Taylor equation [1, Eq. (2.3.1-15); 47, Section 4.2.6]; and (5) used a 30 m square grid over a 125-km^2 model domain (versus 228 km^2 area) (Fig. 12). On the much larger scale of the infiltration map, it is more apparent that infiltration does not occur in ravines with some alluvial fill (since, as previously mentioned, the soil cover and alluvium traps the precipitation and runoff and returns the moisture to the atmosphere through evaporation or plant transpiration), even though a surface weakness in the rock may have been somewhat responsible for the initial formation of the ravine.

A total of 40 infiltration maps were generated for each climate state. Using only a subset of USGS data that could be requalified,

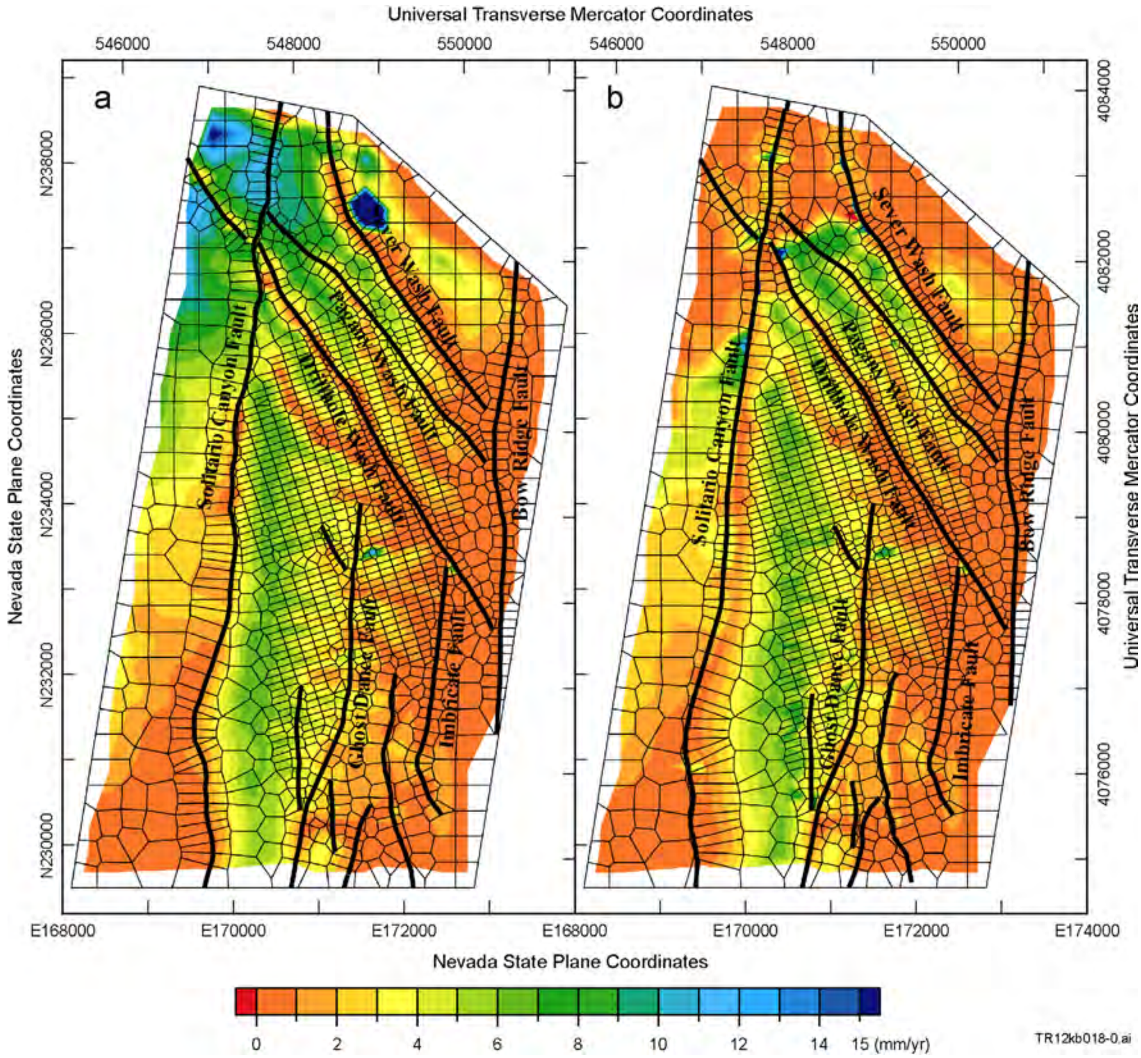

Fig. 13. UZ flow in PA–LA for 10% quantile (62% of simulations) at current, arid conditions [1, Figs. 6.1-2 and 6.6-1] (a) Net infiltration at surface from MASSIF (~3.3 mm/yr over repository area and 3 mm/yr over UZ model domain), and (b) percolation (matrix and fracture flux) at repository.

MASSIF predicted 3 times more net infiltration in the first 10^4 years than PA–SR but values were still less than used in PA–VA (Fig. 5). Hence, the infiltration still centered around the range considered for the wetter climates in PA–EA and PA-93.

The spatial distribution of infiltration was similar to previous PAs (Fig. 13a). The median infiltration at the surface over the 4.6 km^2 repository area was 14 mm/yr. The uncertainty present in the 40 infiltration maps was represented in PA–LA by selecting 4 quantiles to propagate; hence, for the 4 climate states, 16 infiltration maps were selected (i.e., $\overline{q}^{infil}_{w,a}(\mathbf{x})$ where w ~ *arid, monsoon, trans, NRC* and a ~ 10th, 30th, 50th, 90th).

8.2. Percolation in PA–LA

For PA–LA, the basic approach to estimating percolation at the repository level remained the same as in PA–VA and PA–SR (Fig. 9). The 1-D (and 3-D mountain-scale flow meshes discussed below) modeled 32 hydrologic layers (corresponding to 59 mesh layers and 44 stratigraphic layers) between the water table and TCw unit near the surface [6,31,66,78] (Fig. 2).

The calibration consisted of the same 4 steps used in PA–SR using iTOUGH2 v5.0 to produce 4 calibrated infiltration-hydrologic property sets for the 4 infiltration quantiles (h ~10th, 30th, 50th, or 90th) [79]. The 3-D mountain-scale model generated 16 flow fields $q^{perc}_{w,h}$ ($\mathbf{x}$) (product of 4 calibrated infiltration-hydrologic property sets h and 4 climate states w). The mountain scale model, using TOUGH2 v1.6, had a 25% increase in spatial resolution from PA–SR (1.23×10^5 grid blocks, 2042 columns).

Similar to PA–VA and PA–SR but with more data and analysis (e.g., [80]), the reasonableness of the flow fields was examined by comparing measurements in the ESF and enhanced characterization of the repository block (ECRB) of ^{36}Cl, precipitation of calcite in fractures, and temperature profiles. Observed temperatures and ^{36}Cl concentrations agreed best with the 10th quantile infiltration (3.3 mm/year over repository or 3.0 mm/year over UZ model area) and LBNL heavily weighted the probability of the lower values; specifically, $\wp\{\overline{q}^{infil}_{w,a}\} = 0.62, 0.16, 0.16$, and 0.06 for a ~ 10th, 30th, 50th, 90th quantiles, respectively, rather than use a weighting based on the quantiles of 0.2, 0.2, 0.3, and 0.3.[11] The resulting infiltration boundary conditions applied to the UZ flow model were slightly less than for PA–SR (3.3 mm/year versus 4.1 mm/year for $\overline{q}^{infil}_{arid}$) (Fig. 5). Within the repository footprint, the average percolation remained within 3% of the average infiltration for PA–LA (i.e., little lateral flow occurred over the repository, rather most lateral flow occurred to the northwest) (Fig. 13b).

[11] YMP later showed through a sensitivity analysis for the NRC that different weightings did not noticeably influence the dose.

8.3. Seepage in PA–LA

PA–LA again used SCM, SMPA, and SEEPDLL, to determine seepage water volume and number of packages contacted (Fig. 9, Eq. (C)). However improvements were made [6,81]. SCM was calibrated, based on iTOUGH2 v5.0, using liquid release data from locations in both the middle nonlithophysal unit (Tptpmn) in the ESF (Niches 3650, 3107 and 4788) and data in the lower lithophysal unit (Tptpll) (e.g., Niche 1620 along the ECRB).

SMPA developed functions for intact drifts and collapsed drifts after a seismic event for epistemic mean seepage [2, Fig. 6.3.3-5]:

$$\overline{Q}_{v}^{\overset{E}{seep}} = \hbar_{v}^{Q}\{q_f^{perc},\ \overline{k}_f,\ 1/\alpha_f^{van}\}; \text{and}$$

$$\sigma_{v}^{Q^{seep}} = \hbar_{v}^{\sigma}\{q_f^{perc}, \overline{k}_f,\ 1/\alpha_f^{van}\}\ v \sim \text{intact, collapse} \tag{33}$$

For intact drifts ($v \sim intact$), SMPA modeled a quarter of a drift section 4-m wide, 10-m tall normal to the drift axis and 2.44 m along 5.5 m diameter drift using 0.1 m by 0.3 m grid blocks. The functional relationships were determined from 4.8×10^4 simulations (versus 720 in PA–SR), which consisted of 15 values of q_f^{perc} between 1 and 1000 mm/year, 10 values of $1/\alpha_f$ between 100 and 1000 Pa in steps of 100, 16 values of $\overline{k}_f$ between 10^{-14} and 10^{-10}, m^2, and 20 realizations of a conditioned permeability field ($k_f(\mathbf{x})$). Additional simulations were also made to extend the applicable range of the functions. For collapsed drifts ($v \sim collapsed$), SMPA modeled an 11-m diameter drift completely filled with rubble. The functional relationships were determined from 2.4×10^4 simulations, which consisted of the same parametric variation of q_f^{perc}, $\overline{k}_f$ but only 10 realizations of the $k_f(\mathbf{x})$ field.

In addition, distributions for air-entry parameter were developed for lithophysal and nonlithophysal layers (z_{layer}), based on the calibrated values available at 10 different water-release test intervals [81, Table 6.6-1]. A triangular cumulative distribution, based on the standard error of the estimates ($\sigma/\sqrt{n}$), represented epistemic uncertainty for $\Delta 1/\alpha_f^{van}$ $((\mathcal{G}^{tri}(z_{layer}, \Delta(1/\alpha_f^{van}))$. A uniform distribution, based on the standard deviation (σ), represented irreducible aleatoric spatial variability for $1/\alpha_f^{van}$ $((\mathcal{G}^{uni}(z_{layer}, 1/\alpha_f^{van}))$. Distributions for log $\overline{k}_f$were based on the pre-excavation and post-excavation air permeability measurements in the underground. A triangular distribution represented epistemic uncertainty for $\Delta\log\,\overline{k}_f$, and a normal distribution represent aleatoric variability for log $\overline{k}_f$.

To account for heterogeneity below the resolution of the UZ mountain-scale model, the percolation flux was multiplied by a flow focusing factor. The distribution for f^{focus} was based on a 2-D modeling studying conducted with TOUGH2 using smaller element sizes than those for the UZ mountain scale model to account for the intermediate scale heterogeneity. The distribution ranged between 0.116 and 5.016 [81, p. 6–154].[12]

With the functional relationships from SMPA and the distributions for the underlying parameters, the underlying concept for developing a representation of spatially varying seepage, as implemented in SEEPDLL, was more straightforward in PA–LA than in PA–SR [2, Section 6.3.3.1.3 and Fig. 6.3.3-5]. Step 1 for SEEPDLL was to sample the epistemic uncertain parameters $\Delta 1/\alpha_f^{van}$, $\Delta\log\,\overline{k}_f$, and f^{focus}, from their cumulative distributions, once for each realization ℓ (e.g., $\mathcal{G}^{tri}(z_{layer}, \Delta(1/\alpha_{f,\ell}^{van}))$. Step 2 for SEEPDLL was to sample the spatial variability for $1/\alpha_f^{van}$ and log $\overline{k}_f$ from their respective distributions (using two uncorrelated random numbers) (e.g., $\mathcal{G}^{uni}(z_{layer}, 1/\alpha_{f,l}^{van})$) for each of 3264 locations (x_n) and 8 package groups g^{WP} from the thermal-hydrologic $\mathcal{M}^{TH}$ module [8]. Step 3 was to evaluate the intact and collapsed seepage functions at each location x_n and time step (where values only changed when climate changed); for example from Eq. (33), the epistemic mean seepage is

$$\overline{Q}_{v,z,g,h,\ell}^{\overset{E}{seep}}(t,x_n) = \hbar_{v}^{Q}\{(q_{z,g,h,\ell}^{perc}(t,x_n) f_{\ell}^{focus}),$$
$$(\log\overline{k}_{f,z,g,s}(t,x_n) + \Delta\log\overline{k}_{f,z,g,\ell}), \quad (\alpha_{f,z,g,s}^{van}(x_n) + \Delta(1/\alpha_{f,z,g,\ell}^{van}))\} \tag{34}$$

from either drifts $v \sim collapsed\ or\ noncollapsed$, 5 zones z, 8 package groups g, 16 calibrated infiltration-hydrologic property sets h, and 300 samples l at time t and location x_n.

Step 4 was to construct a uniform distribution for both intact and collapsed drifts from, $\overline{Q}_{v,z,g,h,\ell}^{seep^E}(t,x_n)$ and $\sigma_{v,z,g,h,\ell}^{Q^{seep}}(t,x_n)$ (recall, PA–VA and PA–SR used a beta distribution) and sample using an uncorrelated random number $u_s^{seep}[0,1]$ to obtain spatially variable $Q_{v,z,g,h,\ell}^{seep}(t,x_n)$ where $v \sim intact\ or\ collapsed$. Step 5 was to increase the intact seepage $Q_{intact,z,g,\ell}^{seep}(t,x_n)$ by 20% to include possibility of partial drift collapse from a seismic event (based on calculations with UDEC, 3DEC, and FLAC3D—Fig. 9c [7, Fig. 7]. Furthermore, seepage was set to zero whenever the drift wall temperature $T_{g,h,\alpha^{thermal}}^{drift}(t,\mathbf{x})$, as calculated by $\mathcal{M}^{TH}$ at a waste package group g, hydrologic calibration h, and thermal conductivity $\alpha^{thermal}$ [8], was above a threshold of 100 °C. This threshold was based on modeling studies of the heater tests conducted at Yucca Mountain [62,71,82,83]. Step 6 was to evaluate the fraction of packages with seepage above a threshold of 0.1 kg/year per package, which designated a dripping environment $f_{z,g,\ell}^{WPdrip}$. Also, seepage based on 2 WP types p was estimated from the seepage for the 8 package groups g and a zone average seepage was calculated ($\overline{Q}_{v,p,z,d,\ell}^{seep}(t)$ for use in $\mathcal{M}^{Waste}$ and $\mathcal{M}^{EBStrans}$ [7, Fig. 7; 26].

9. Summary

Scientific understanding of infiltration in a desert environment, unsaturated flow in fractures, and seepage into an open drift in a thermally perturbed environment was initially lacking in 1984, and, thus YMP expended much effort in developing this understanding and how to adequately model this phenomena. As understanding of the YM disposal system increased through site characterization and *in situ* testing, modeling of infiltration, percolation, and seepage evolved from simple assumptions in a single model in 1984 to three modules ($\mathcal{M}^{Infil}$, $\mathcal{M}^{UZflow}$, and $\mathcal{M}^{Seep}$) each based on several detailed process models by PA–VA in 1998. These modules were then further refined by PA–LA in 2008 (Fig. 2).

Introduced in PA-91, $\mathcal{M}^{UZflow}$ evaluated 1-D vertical percolation in the unsaturated zone below the repository, based on a single equivalent continuum model (ECM), with flow primarily in the matrix. However, both PA-91 and PA-93 also considered a weep alternative conceptual model of flow solely in the fractures. PA-95 used 1-D results of percolation from an ECM formulation from the surface. PA–VA was the first to incorporate results of percolation through dual permeability media (both fractures and the matrix) in a 3-D model grid from the surface to the water table. Further refinements in $\mathcal{M}^{UZflow}$ after PA–VA included more detailed model grids and more extensive calibration. Uncertainty in percolation through the fractured volcanic tuff of Yucca Mountain was usually important in explaining the observed uncertainty in the performance measure (cumulative release in PA–EA, PA-91, and PA-93 and individual dose, thereafter).

[12] Percolation had also been focused in PA–SR but used a different method to evaluate f^{focus}, which resulted in potentially larger values of f^{focus} [29, Section 3.9.6.3].

An important step for incorporating percolation from the surface was to develop an infiltration boundary condition, and, thus, an infiltration module $\mathcal{M}^{Infil}$ was added in PA–VA (Fig. 2). Refinements for PA–LA included improving descriptions of uncertainty and evaluating evapotranspiration using international guidelines. Also until PA–VA, evaluating seepage in the disposal drift was fairly rudimentary. The seepage module $\mathcal{M}^{Seep}$, introduced for PA–VA, included a detailed, calibrated model of a drift and development of seepage functions for use in the PA from numerous simulations. Refinements for PA–LA included separating uncertainty and variability in seepage and much more elaborate calibration. Generally, little water reaches the repository horizon under current climate conditions, and then in only small areas connected by fractures. Yet, high infiltration and percolation at the repository horizon was usually considered for a portion of the regulatory period in all PAs, to evaluate the influence of fluctuations in climate on disposal system performance (Fig. 5).

Acknowledgments

Sandia National Laboratories (SNL) is a multi-program laboratory operated by Sandia Corporation, a wholly owned subsidiary of Lockheed Martin Corporation, for the DOE National Nuclear Security Administration under contract DE-AC04-94AL85000. The authors wish to thank L.A. Connolly, SNL, for help with references, and S.K. Best, Raytheon, for illustration support. The historical perspective and opinions presented are those of the authors and are not necessarily those held by reviewers, SNL, or DOE. As a historical perspective, the authors are reporting on the work of others; however, any interpretative errors of documentation are those of the authors alone. Each performance assessment discussed in this paper required numerous participants with expertise in many areas of science and technology. The most complete listing of these participants is made by examining the extensive reference list. However, many of references are corporate documents without authors. Furthermore, the extensive time some scientists and engineers devoted to UZ flow modeling and the handoff between different scientists and engineers as YMP transitioned through four study phases (site identification, feasibility analysis, suitability analysis, and compliance analysis [6, Table 1] is more evident if acknowledged here in somewhat chronological order. Specifically, contributors to the analysis of UZ flow include R.R. Peters, SNL and E.A. Klavetter, SNL (early modeling of UZ flow with TOSPAC for PA–EA [19] and SCP [20]); K. Pruess, LBNL (TOUGH2 development [53]); J.H. Gauthier, SNL (UZ flow analysis for PA–EA [19], PA-91 [14], PA-93 [15], PA–VA, and PA–SR); M.L. Wilson, SNL (UZ flow analysis for PA-91, PA-93, and PA–VA [30], seepage abstraction for PA–SR); R.R. Eaton, SNL (UZ flow analysis for PA-91 [14] and PA-93 [15]); G.S. Bodvarsson, LBNL (development of UZ flow process modeling team, conceptual flow model development, and analysis for PA-95 [43], PA–VA [52], and PA–SR [29]); T.M. Bandurraga, LBNL (conceptual flow model and calibration for PA–VA [58]); C.F. Ahlers, LBNL (calibration of flow properties in PA–VA [57] and PA–SR [68]); Y-S. Wu, LBNL now at Colorado School of Mines (modeling and analysis for PA–VA [51], PA–SR [71], and PA–LA [67]); E.L. Sonnenthal, LBNL (consistency of geochemistry with modeling for PA–VA [60]); J. Hinds, LBNL (ESF data analysis for PA–VA [52] and numerical grids for PA–SR [69] and PA–LA); H-H. Liu, LBNL (active fracture model [55] for PA–SR and thereafter, and calibration of UZ flow properties for PA–LA [79]); L. Pan, LBNL (numerical grids for PA–SR [69] and hydrologic properties for PA–LA [80]); P. Dobson, LBNL (numerical grids for PA–SR and PA–LA); C.K. Ho, SNL (PA lead on UZ flow for PA–VA [30], PA–SR [29], and PA–LA); D.A. Chesnut, LLNL (seepage abstraction for PA-91 [38] and PA-93); J.T. Birkholzer, LBNL (seepage testing for PA–VA [61] and PA–SR [82] and abstraction PA–LA [81]. Several USGS geologists contributed to modeling infiltration for PA–VA [46] and PA–SR [23]: A. Flint, J.A. Hevesi, and L. Flint. For PA–LA, J. Stein, SNL led the team evaluating infiltration [24]. USGS and LBNL geoscientists also contributed much to characterizing the UZ as noted in a companion paper [5]. Because so many scientists and engineers were involved in evaluating UZ flow at YMP, the authors recognize that this list is unavoidably incomplete, and we apologize for omissions and oversights.

References

[1] DOE (US Department of Energy). Yucca Mountain repository license application, safety analysis report. DOE/RW-0573. Washington, DC: Office of Civilian Radioactive Waste Management, US Department of Energy; 2008.
[2] Sandia National Laboratories (SNL). Total system performance assessment model/analysis for the license application. MDL-WIS-PA-000005. Las Vegas, NV: Sandia National Laboratories; 2008.
[3] Rechard RP, Cotton TA, Voegele M. Site selection and regulatory basis for the Yucca Mountain disposal system for spent nuclear fuel and high-level radioactive waste. Reliability Engineering and System Safety; http://dx.doi.org/10.1016/j.ress.2013.06.021, this issue.
[4] Rechard RP, Freeze GA, Perry FV. Hazards and scenarios examined for the Yucca Mountain disposal system for spent nuclear fuel and high-level radioactive waste. Reliability Engineering and System Safety; http://dx.doi.org/10.1016/j.ress.2013.06.014, this issue.
[5] Rechard RP, Voegele MD. Evolution of repository and package designs for Yucca Mountain disposal system for spent nuclear fuel and high-level radioactive waste. Reliability Engineering and System Safety; http://dx.doi.org/10.1016/j.ress.2013.06.018, this issue.
[6] Rechard RP, Liu HH, Tsang YW, Finsterle S. Site characterization of the Yucca Mountain disposal system for spent nuclear fuel and high-level radioactive waste. Reliability Engineering and System Safety; http://dx.doi.org/10.1016/j.ress.2013.06.021, this issue.
[7] Rechard RP, Wilson ML, Sevougian SD. Progression of performance assessment modeling for the Yucca Mountain disposal system for spent nuclear fuel and high-level radioactive waste. Reliability Engineering and System Safety; http://dx.doi.org/10.1016/j.ress.2013.06.026, this issue.
[8] Rechard RP, Lee JH, Hardin E, Bryan CR. Waste package degradation from thermal and chemical processes in performance assessments of the Yucca Mountain disposal system for spent nuclear fuel and high-level radioactive waste. Reliability Engineering and System Safety; http://dx.doi.org/10.1016/j.ress.2013.06.027, this issue.
[9] Rechard RP, Arnold BW, Robinson BA, Houseworth JE. Transport modeling in performance assessments for the Yucca Mountain disposal system for spent nuclear fuel and high-level radioactive waste. Reliability Engineering and System Safety; http://dx.doi.org/10.1016/j.ress.2013.06.031, this issue.
[10] Rechard RP. Results from past performance assessments of the Yucca Mountain disposal system for spent nuclear fuel and high-level radioactive waste. Reliability Engineering and System Safety; http://dx.doi.org/10.1016/j.ress.2013.06.030, this issue.
[11] Morgan MG, Henrion M. Uncertainty: a guide to dealing with uncertainty in quantitative risk and policy analysis. New York, NY: Cambridge University Press; 1990.
[12] Sinnock S, Lin YT, Brannen JP. Preliminary bounds on the expected postclosure performance of the Yucca Mountain repository site, southern Nevada. SAND84-1492. Albuquerque, NM: Sandia National Laboratories; 1984.
[13] Sinnock S, Lin YT, Brannen JP. Preliminary bounds on the expected postclosure performance of the Yucca Mountain repository site, southern Nevada. Journal of Geophysical Research 1987;92(B8):7820–42.
[14] Barnard RW, Wilson ML, Dockery HA, Gauthier JH, Kaplan PG, Eaton RR, et al. TSPA 1991: an initial total-system performance assessment for Yucca Mountain. SAND91-2795. Albuquerque, NM: Sandia National Laboratories; 1992.
[15] Wilson ML, Gauthier JH, Barnard RW, Barr GE, Dockery HA, Dunn E, et al. Total-system performance assessment for Yucca Mountain—SNL second iteration (TSPA-1993). Executive summary and two volumes. SAND93-2675. Albuquerque, NM: Sandia National Laboratories; 1994.
[16] Atkins JE, Andrews RW, Duguid JO, Dunlap BE, Houseworth JE, Kennedy LR, et al. Total system performance assessment—1995: an evaluation of the potential Yucca Mountain Repository. B00000000-01717-2200-00136 REV 01. Las Vegas, NV: Civilian Radioactive Waste Management System Management and Operating Contractor; 1995.
[17] DOE (US Department of Energy). Viability assessment of a repository at Yucca Mountain. DOE/RW-0508. Washington, DC: Office of Civilian Radioactive Waste Management, US Department of Energy; 1998.
[18] DOE (US Department of Energy). Yucca Mountain science and engineering report. DOE/RW-0539. Las Vegas, NV: Office of Civilian Radioactive Waste Management, US Department of Energy; 2001.
[19] Peters RR, Gauthier JH. Results of TOSPAC hydraulic calculations for Yucca Mountain, memorandum to F.W. Bingham, April 30, 1984. Albuquerque, NM: Sandia National Laboratories; 1984.

[20] Klavetter EA, Peters RR. Estimation of hydrologic properties of an unsaturated, fractured rock mass. SAND-84-2642. Albuquerque, NM: Sandia National Laboratories; 1986.
[21] Waddell RK. Two-dimensional, steady-state model of ground-water flow, Nevada Test Site and vicinity, Nevada—California. Water-Resources Investigations Report 82-4085. Denver, CO: US Geological Survey; 1982.
[22] Montazer P, Wilson WE. Conceptual hydrologic model of flow in the unsaturated zone, Yucca Mountain, Nevada. Water-Resources Investigations Report 84-4345. Lakewood, CO: US Geological Survey; 1984.
[23] Flint AL, Flint LE, Bodvarsson GS, Kwicklis EM, Fabryka-Martin J. Evolution of the conceptual model of unsaturated zone hydrology at Yucca Mountain, Nevada. Journal of Hydrology 2001;247(1–2):1–30.
[24] Stein JS. Simulation of net infiltration for present-day and potential future climates. MDL-NBS-HS-000023 REV 01 ADD 01. Las Vegas, NV: Sandia National Laboratories; 2008.
[25] Tyler LD, Zimmerman RM, Langkopf BS, Johnstone JK, Erdal BR, Friedman AM. Field experiment program for tuff in G-Tunnel. In: Proceedings of the1980 national waste terminal storage program information meeting, Columbus, OH, December 9–11, 1980. Columbus, OH: Office of Nuclear Waste Isolation, Battelle Memorial Institute; 1980.
[26] Rechard RP, Stockman CT. Waste degradation and mobilization in performance assessments of the Yucca Mountain disposal system for spent nuclear fuel and high-level radioactive waste. Reliability Engineering and System Safety, http://dx.doi.org/10.1016/j.ress.2013.06.028, this issue.
[27] Prindle RW, Hopkins PL. On conditions and parameters important to model sensitivity for unsaturated flow through layered, fractured tuff: results of analyses for HYDROCOIN level 3 case 2. SAND89-0652. Albuquerque, NM: Sandia National Laboratories; 1990.
[28] Rechard RP, Tierney MS. Assignment of probability distributions for parameters in the 1996 performance assessment for the Waste Isolation Pilot Plant, Part 2: application of process. Reliability Engineering and System Safety 2005;88(1):33–80.
[29] Bodvarsson GS, Ahlers CF, Cushey M, Dove FH, Finsterle SA, Haukwa CB, et al. Unsaturated zone flow and transport model process model report. TDR-NBS-HS-000002, REV 00. Las Vegas, NV: Civilian Radioactive Waste Management System Management and Operating Contractor; 2000.
[30] Ho CK, Wilson ML, Altman SJ. Unsaturated zone hydrology model. Chapter 2 of total system performance assessment-viability assessment (TSPA–VA) analyses technical basis document. B00000000-01717-4301-00002 REV 01. Las Vegas, NV: Civilian Radioactive Waste Management System Management and Operating Contractor; 1998.
[31] Sandia National Laboratories (SNL). UZ flow models and submodels. MDL-NBS-HS-000006 REV 03 AD 01. Las Vegas, NV: Sandia National Laboratories; 2007.
[32] US Nuclear Regulatory Commission (NRC). Implementation of a dose standard after 10,000 years; proposed rule. Federal Register 2005;70(173):53313–20.
[33] Dudley AL, Peters RR, Gauthier JH, Wilson ML, Tierney MS, Klavetter EA. Total system performance assessment code (TOSPAC): Volume 1, physical and mathematical bases: Yucca Mountain Project. SAND85-0002. Albuquerque, NM: Sandia National Laboratories; 1988.
[34] Pruess K, Wang JSY, Tsang YW. On thermohydrologic conditions near high-level nuclear wastes emplaced in partially saturated fractured tuff: 2. Effective continuum approximation. Water Resources Research 1990;26(6):1249–61.
[35] Freeze RA, Cherry JA. Groundwater. Englewood Cliffs, NJ: Prentice-Hall; 1979.
[36] Barnard RW, Dockery HA. Nominal configuration, hydrogeologic parameters and calculational results. Volume 1 of technical summary of the performance assessment calculational exercises for 1990 (PACE-90). SAND90-2726. Albuquerque, NM: Sandia National Laboratories; 1991.
[37] Gauthier JH, Wilson ML, Lauffer FC. Estimating the consequences of significant fracture flow at Yucca Mountain high-level radioactive waste management. In: Proceedings of the third annual international conference, Las Vegas, NV, April 12–16, 1992. La Grange Park, IL: American Nuclear Society; 1992: p. 891–8.
[38] Chesnut DA. Characterizing the altered zone at Yucca Mountain: the beginning of a testing strategy. In: Proceedings of the third annual international conference on high-level radioactive waste management, Las Vegas, NV. La Grange Park, IL: Americal Nuclear Society; 1992: p. 1026–39.
[39] Sandia National Laboratories (SNL). EBS radionuclide transport abstraction. ANL-WIS-PA-000001 REV 03, ACC: DOC.20071004.0001. Las Vegas, NV: Sandia National Laboratories; 2007.
[40] Wilson ML. Sensitivity analyses for total-system performance assessment. In: Proceedings of the fourth international conference on high level radioactive waste management, Las Vegas, NV, April 26–30, 1993. La Grange Park, IL: American Nuclear Society, 1993; vol. 1: p. 14–21.
[41] Nuclear Waste Technical Review Board (NWTRB). Report to the US Congress and the US Secretary of Energy, 1995 findings and recommendations. Arlington, VA: Nuclear Waste Technical Review Board; 1996.
[42] Flint LE, Flint AL. Spatial distribution of potential near surface moisture flux at Yucca Mountain. In: Proceedings of the fifth annual international conference on high-level radioactive waste management, Las Vegas, NV, May 22–26, 1994. La Grange Park, IL: American Nuclear Society; 1994: p. 23522–8.
[43] Wittwer C, Chen G, Bodvarsson GS, Chornack M, Flint A, Flint L, et al. Preliminary development of the LBL/USGS three-dimensional site-scale model of Yucca Mountain, Nevada. LBL-37356. Berkeley, CA: Lawrence Berkeley Laboratory; 1995.
[44] Hevesi JA, Ambos DS, Flint AL. Simulation of net infiltration for modern and potential future climates. MDL-NBS-HS-000023 REV 00. Las Vegas, NV: Civilian Radioactive Waste Management System Management and Operating Contractor; 2000.
[45] Adams M. Yucca Mountain—Nevada's perspective. Idaho Law Review 2010;46:1–26.
[46] Flint AL, Hevesi JA, Flint LE. Conceptual and numerical model of infiltration for the Yucca Mountain area, Nevada. Milestone 3GUI623M. Denver, CO: US Geological Survey; 1996.
[47] Shuttleworth JW. Evaporation. In: Maidment DR, editor. Handbook of Hydrology. New York, NY: McGraw Hill; 1992.
[48] Winograd IJ. Radioactive waste storage in the arid zone. EOS, Transactions American Geophysical Union 1974;55(10):834–94.
[49] Winograd IJ. Radioactive waste disposal in thick unsaturated zones. Science 1981;212(4502):1457–64.
[50] Cochran JR, Beyeler WE, Brosseau DA, Brush LH, Brown TJ, Crowe BM, et al. Compliance assessment document for the transuranic wastes in the greater confinement disposal boreholes at the Nevada Test Site, Volume 2: performance assessment. SAND2001-2977. Albuquerque, NM: Sandia National Laboratories; 2001.
[51] Wu Y-S, Haukwa C, Bodvarsson GS. A site-scale model for fluid and heat flow in the unsaturated zone of Yucca Mountain, Nevada. Journal of Contaminant Hydrology 1999;38(1–3):185–215.
[52] Bodvarsson GS, Bandurraga TM, Wu YS. The site-scale unsaturated zone model of Yucca Mountain, Nevada, for the viability assessment. LBNL-40376. Berkeley, CA: Lawrence Berkeley National Laboratory; 1997.
[53] Pruess K. TOUGH2: a general-purpose numerical simulator for multiphase fluid and heat flow. LBL-29400. Berkeley, CA: Lawrence Berkeley National Laboratory; 1991.
[54] Wu Y-S. UZ flow models and submodels. MDL-NBS-HS-000006 REV 00. Las Vegas, NV: Civilian Radioactive Waste Management System Management and Operating Contractor; 2000.
[55] Liu HH, Doughty C, Bodvarsson GS. An active fracture model for unsaturated flow and transport in fractured rocks. Water Resources Research 1998;34(10):2633–46.
[56] Finsterle S. ITOUGH2 user's guide version 2.2. LBNL-34581. Berkeley, CA: Lawrence Berkeley National Laboratory; 1993.
[57] Ahlers CF, Finsterle S, Bodvarsson GS. Characterization of subsurface pneumatic response at Yucca Mountain. Journal of Contaminant Hydrology 1999;38(1–3):47–68.
[58] Bandurraga YM, Bodvarsson GS. Calibrating hydrogeologic parameters for the 3-D site-scale unsaturated zone model of Yucca Mountain, Nevada. Journal of Contaminant Hydrology 1999;38(1–3):25–46.
[59] Sevougian SD. Summary and conclusions. Chapter 11 of total system performance assessment-viability assessment (TSPA–VA) analyses technical basis document. B00000000-01717-4301-00011 REV 01. Las Vegas, NV: Civilian Radioactive Waste Management System Management and Operating Contractor; 1998.
[60] Sonnenthal EL, Bodvarsson GS. Constraints on the hydrology of the unsaturated zone at Yucca Mountain, NV from three-dimensional models of chloride and strontium geochemistry. Journal of Contaminant Hydrology 1999; 38(1–3):107–56.
[61] Birkholzer J, Li G, Tsang C-F, Tsang Y. Modeling studies and analysis of seepage into drifts at Yucca Mountain. Journal of Contaminant Hydrology 1999; 38(1–3):349–84.
[62] Birkholzer JT, Tsang YW. Modeling the thermal-hydrologic processes in a large-scale underground heater test in partially saturated fractured tuff. Water Resources Research 2000;36(6):1431–47.
[63] Deutsch CV, Journel AG. GSLIB geostatistical software library and user's guide. New York, NY: Oxford University Press; 1992.
[64] US Nuclear Regulatory Commission (NRC). Disposal of high-level radioactive wastes in a proposed geological repository at Yucca Mountain, Nevada; proposed rule. Federal Register 1999;64:8640–79.
[65] Bechtel SAIC Company (BSC). Future climate analysis. ANL-NBS-GS-000008 REV 01. Las Vegas, NV: Bechtel SAIC Company; 2004.
[66] Wu Y-S, Zhang W, Bodvarsson GS. A mountain-scale model for characterizing unsaturated flow and transport in fractured tuffs of Yucca Mountain. Vadose Zone Journal 2004;3:796–805.
[67] Wu Y-S, Zhang W, Bodvarsson GS. Analyzing unsaturated flow patterns in fractured rock using an integrated modeling approach. Hydrogeology Journal 2007;15:553–72.
[68] Ahlers C, Liu H. Calibrated properties model. MDL-NBS-HS-000003 REV 00. Las Vegas, NV: Civilian Radioactive Waste Management System Management and Operating Contractor; 2000.
[69] Hinds J, Pan L. Development of numerical grids for UZ flow and transport modeling. ANL-NBS-HS-000015 REV 00. Las Vegas, NV: Civilian Radioactive Waste Management System Management and Operating Contractor; 2000.
[70] Civilian Radioactive Waste Management System (CRWMS). Total system performance assessment for the site recommendation. TDR-WIS-PA-000001 REV 00, ICN 01. Las Vegas, NV: Civilian Radioactive Waste Management System Management and Operating Contractor; 2000.
[71] Wu Y-S, Pan L, Zhang W, Bodvarsson GS. Characterization of flow and transport processes within the unsaturated zone of Yucca Mountain, Nevada, under current and future climates. Journal of Contaminant Hydrology 2002;54:215–47.
[72] Bechtel SAIC Company (BSC). UZ flow models and submodels. MDL-NBS-HS-000006 REV 02. Las Vegas, NV: Bechtel SAIC Company; 2004.

[73] Finsterle S, Ahlers CF, Trautz RC, Cook PJ. Inverse and predictive modeling of seepage into underground openings. Journal of Contaminant Hydrology 2003;62–63:89–109.
[74] Wang JSY, Trautz RC, Cook PJ, Finsterle S, James AL, Birkholzer JT. Field tests and model analyses of seepage into drifts at Yucca Mountain. Journal of Contaminant Hydrology 1999;38(1–3):323–48.
[75] Mattie PS, Miller SP. Total system performance assessment (TSPA) model for site recommendation. MDL-WIS-PA-000002 REV 00. Las Vegas, NV: Civilian Radioactive Waste Management System Management and Operating Contractor; 2000.
[76] US Environmental Protection Agency (EPA). 40 CFR Part 197: public health and environmental radiation protection standards for Yucca Mountain, Nevada; proposed rule. Federal Register 2005;70(161):49014.
[77] Nuclear Waste Technical Review Board (NWTRB). Letter report to the US Congress and the Secretary of Energy; January 2007. Arlington, VA: Nuclear Waste Technical Review Board; 2007.
[78] Liu HH, Zhang G, Bodvarsson GS. The active fracture model: its relation to fractal flow behavior and a further evaluation using field observations. Vadose Zone Journal 2003;2:259–69.
[79] Liu HH. Calibrated unsaturated zone properties. ANL-NBS-HS-000058, REV 00. Las Vegas, NV: Sandia National Laboratories; 2007.
[80] Pan L. Analysis of hydrologic properties data. ANL-NBS-HS-000042 REV 0. Las Vegas, NV: Bechtel SAIC Company; 2004.
[81] Birkholzer JT. Abstraction of drift seepage. MDL-NBS-HS-000019, REV 01. ADD 01. Las Vegas, NV: Bechtel SAIC Company; 2007.
[82] Birkholzer JT, Mukhopadhyay S, Tsang YW. Modeling seepage into heated waste emplacement tunnels in unsaturated fractured rock. Vadose Zone Journal 2004;3(3):819–36.
[83] Birkholzer JT, Mukhopadhyay S, Tsang YM. The impact of preferential flow on the vaporization barrier above waste emplacement drifts of. Yucca Mountain Nuclear Technology 2004;148(2):138–50.